

Accessibility of Different Histone H3-Binding Domains of UHRF1 Is Allosterically Regulated by Phosphatidylinositol 5-Phosphate

Kathy A. Gelato,¹ Maria Tauber,¹ Michelle S. Ong,² Stefan Winter,¹ Kyoko Hiragami-Hamada,¹ Julia Sindlinger,³ Alexander Lemak,⁴ Yvette Bultsma,^{5,6} Scott Houlston,^{2,4} Dirk Schwarzer,³ Nullin Divecha,^{5,6} Cheryl H. Arrowsmith,^{2,4} and Wolfgang Fischle^{1,*}

¹Laboratory of Chromatin Biochemistry, Max Planck Institute for Biophysical Chemistry, Am Fassberg 11, 37077 Göttingen, Germany

²Structural Genomics Consortium, University of Toronto, 101 College Street, Toronto, ON M5G 1L7, Canada

³Interfaculty Institute of Biochemistry, University of Tübingen, Hoppe-Seyler-Strasse 4, 72076 Tübingen, Germany

⁴Princess Margaret Cancer Center, TMDT, 101 College Street, Toronto, ON M5G 1L7, Canada

⁵Cancer Research UK Manchester Institute, The University of Manchester, Wilmslow Road, Manchester M20 4BX, UK

⁶Present address: Centre for Biological Sciences, University of Southampton, Life Sciences Building 85, Highfield, Southampton SO17 1BJ, UK

*Correspondence: wfischl@gwdg.de

<http://dx.doi.org/10.1016/j.molcel.2014.04.004>

SUMMARY

UHRF1 is a multidomain protein crucially linking histone H3 modification states and DNA methylation. While the interaction properties of its specific domains are well characterized, little is known about the regulation of these functionalities. We show that UHRF1 exists in distinct active states, binding either unmodified H3 or the H3 lysine 9 trimethylation (H3K9me3) modification. A polybasic region (PBR) in the C terminus blocks interaction of a tandem tudor domain (TTD) with H3K9me3 by occupying an essential peptide-binding groove. In this state the plant homeodomain (PHD) mediates interaction with the extreme N terminus of the unmodified H3 tail. Binding of the phosphatidylinositol phosphate PI5P to the PBR of UHRF1 results in a conformational rearrangement of the domains, allowing the TTD to bind H3K9me3. Our results define an allosteric mechanism controlling heterochromatin association of an essential regulatory protein of epigenetic states and identify a functional role for enigmatic nuclear phosphatidylinositol phosphates.

INTRODUCTION

A major concept that has emerged for the readout of histone modifications is the recruitment of proteins containing conserved domains that specifically interact with defined modifications. Systematic proteomic approaches have implied that individual chromatin modifications are usually recognized by multiple competing proteins (Patel and Wang, 2013). To understand the readout of chromatin marks, it is therefore imperative to dissect how the interplay between modifications and binding factors is regulated. The exact context appears to matter, as

neighboring modifications can influence interaction in a negative or positive manner. Posttranslational modifications of chromatin-associated proteins can directly affect the modification binding properties of chromatin proteins. Further, the expression of specific binding factors is modulated in cell differentiation and development (reviewed by Fischle, 2012).

Since transient changes in cellular states (e.g., nutrition levels) can have a lasting effect on gene expression patterns, it has been suggested that metabolites and small cellular molecules have an immediate impact on the condition of chromatin and the epigenetic state of cells (Lu and Thompson, 2012). Phosphatidylinositol phosphates (PIPs) are particularly interesting in the context of chromatin. A pool of these lipids exists in the cell nucleus, separately regulated from the cell membrane and cytoplasm by dedicated enzymes. However, the exact biochemical state of PIPs in this compartment is still unclear (Barlow et al., 2010; Fiume et al., 2012). The bulk of nuclear phospholipids copurifies with nonhistone chromosomal proteins (Manzoli et al., 1976). Interestingly, analysis of isolated chromatin fractions revealed that lipids associated with hetero- and euchromatin each showed distinct turnover rates (Rose and Frenster, 1965). Furthermore, hydrolysis of nuclear phospholipids by phospholipase C (PLC) was shown to change chromatin structure (Maraldi et al., 1984).

Few nuclear proteins have been found to associate with PIPs so far (Barlow et al., 2010; Fiume et al., 2012). PI4,5P₂ has been shown to activate and stabilize the chromatin remodeling complex BAF (Burgio et al., 2010). The H3K4me3-binding plant homeodomain (PHD) and adjacent polybasic region of ING2 and several related proteins associate with chromatin through a PI5P-mediated mechanism (Bua and Bindra, 2009; Gozani et al., 2003; Jones et al., 2006). While this pathway is important in controlling ING2-dependent genes, especially in DNA damage pathways, interaction of H3K4me3 and PI5P are independent of each other (Bua et al., 2013). Binding of PI5P to a PHD domain causes ATX1 to detach from promoters and translocate from the nucleus to the cytosol (Ndamukong et al., 2010). Whereas major biochemical screens have been conducted for PIP-binding factors in the cytoplasmic fraction (Catimel et al., 2009;

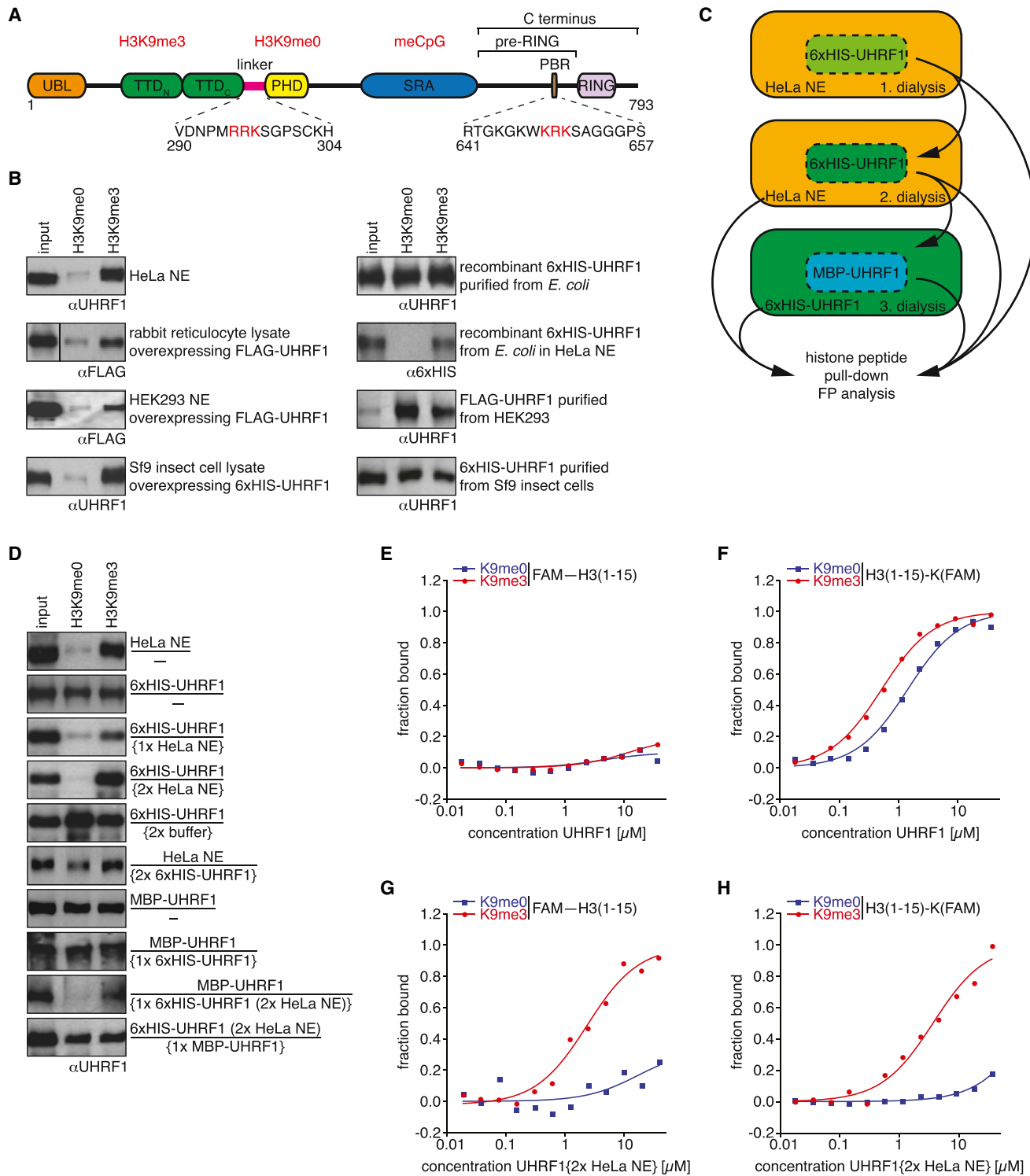


Figure 1. UHRF1 Binding to the Modified or Unmodified H3 Tail Is Regulated by Cellular Cofactors

(A) Domain structure of UHRF1. UBL, ubiquitin-like (aa 1–76); TTD, tandem tudor domain (aa 126–285); PHD, plant and homeodomain (aa 310–366); SRA, SET- and RING-associated (aa 435–586); PBR, polybasic region; RING, really interesting new gene (aa 724–763).

(B) Cellular lysates (NE, nuclear extract) and purified cellular or recombinant proteins were incubated with the specified biotinylated H3(1–20) peptides immobilized on streptavidin magnetic beads. Recovered material was analyzed by western blot. Input, 2%.

(C) Flow scheme for dialysis experiments as analyzed in (D)–(H).

(legend continued on next page)

Pasquali et al., 2007), only one study attempted to define the nuclear interactome of a PIP, namely PI4,5P₂. There, lysine/arginine-rich patches with the consensus K/R-(X)_n = 3–7-K-X-K/R-K/R emerged as major interaction motifs (Lewis et al., 2011).

Ubiquitin-like with PHD and RING finger domains 1 (UHRF1), also known as inverted CCAAT box protein of 90 kDa (ICBP90) and NP95 in mouse, is a nuclear multidomain factor implicated in the maintenance of DNA methylation patterns during replication. Deletion of *UHRF1* in mice is embryonic lethal. The knockout embryonic stem cells show loss of DNA methylation, enhanced susceptibility to DNA replication arrest, increased sensitivity to DNA damaging agents, impaired maintenance of higher-order chromatin structure, and spurious transcription of repetitive DNA elements (Bostick et al., 2007; Sharif et al., 2007). *UHRF1* is upregulated in various cancer cells, including breast, prostate, and lung cancer, where it plays a key role in promoting proliferation (Bronner et al., 2010).

UHRF1 is composed of at least five domains: an N-terminal ubiquitin-like domain (UBL), followed by a tandem tudor domain (TTD), a plant homeodomain (PHD), a SET and RING-associated (SRA) domain, and a C-terminal really interesting new gene (RING) domain (Figure 1A). The SRA domain preferentially binds to hemimethylated CpG, which during semiconservative replication of DNA recruits DNMT1 to copy the methylation pattern onto the daughter strand (Berkyurek et al., 2014; Rottach et al., 2010; Sharif and Koseki, 2011). This process appears to also involve H3K23 ubiquitylation by the RING (Nishiyama et al., 2013). The isolated TTD binds H3K9me3 (Nady et al., 2011), while the isolated PHD recognizes the unmodified extreme H3 N terminus (Rajakumara et al., 2011). Functional cooperation by these modules was recently suggested by structural and functional studies on isolated TTD-PHD fragments (Arita et al., 2012; Cheng et al., 2013; Rothbart et al., 2013). Both DNA methylation and H3K9me3 are hallmarks of pericentric heterochromatin where *UHRF1* is preferentially localized (Liu et al., 2013). *UHRF1* is also found in euchromatin and regulates gene expression, particularly the silencing of tumor suppressor genes, possibly through affecting DNA methylation and histone modifications (Bronner et al., 2010; Wang et al., 2012). Posttranslational modification of *UHRF1* has been implicated in regulating its stability and possibly directing its interaction with chromatin components (Arita et al., 2012; Ma et al., 2012).

While the interactions of many histone modification-binding domains with their target sites are well studied, it is not always clear if and how the findings on the isolated modules pertain to the proteins and complexes containing them. Here, we analyzed the histone modification binding properties of intact, full-length *UHRF1*. We found that the protein is allosterically regulated for

interaction with unmodified H3 versus H3K9me3, principally by PI5P, which controls access to the TTD and PHD domains. Our results imply that this mechanism contributes to directing *UHRF1* heterochromatin localization and function.

RESULTS

UHRF1 Exists in Different Functional States

To obtain insights into the recognition of histone marks by *UHRF1*, we performed histone peptide pull-down experiments using the lysate or purified form of the FLAG- or 6×HIS-tagged protein from different expression systems. Endogenous *UHRF1* in HeLa cell nuclear extract (NE) exhibited preference for H3K9me3 over the unmodified form (H3K9me0) (Figure 1B). Similar binding specificity was observed for *UHRF1*-FLAG in vitro translated in rabbit reticulocyte extract or in NE prepared from HEK293 cells overexpressing the fusion protein and for 6×HIS-UHRF1 in total lysate of Sf9 insect cells programmed for expression. In contrast, recombinant 6×HIS-UHRF1 from *E. coli* bound the H3K9me0 and H3K9me3 states equally well. Similarly, the *UHRF1*-FLAG or 6×HIS-UHRF1 proteins affinity purified from the overexpressing human embryonic kidney 293 (HEK293) or Sf9 cell extracts, respectively, displayed comparable interaction with both H3 tail peptides. Bacterial, recombinant 6×HIS-UHRF1 preferentially bound H3K9me3 when put into HeLa NE. As we observed distinct behavior in multiple expression systems and with different affinity tags at the N and C terminus, we concluded that the proteins in the NE and those that are affinity purified likely exist in different functional states.

UHRF1 Interaction with the Modified or Unmodified H3 Tail Is Regulated by Cellular Cofactors

Similar to previous findings (Nady et al., 2011), we observed that the isolated TTD of *UHRF1* specifically binds to H3K9me3 (Figure S1A available online). In contrast, the PHD domain interacted with the extreme H3 tail irrespective of the modification status of the K9 site (Hu et al., 2011; Lallous et al., 2011; Rajakumara et al., 2011; Wang et al., 2011). This behavior was reflected in quantitative fluorescence polarization binding experiments (FP). We used two sets of peptides corresponding to residues 1–15 of the H3 tail with fluorescein attached to either the N or C terminus. Both types of peptides carrying the K9me3 mark bound to the TTD with similar affinity, while no interaction with the unmodified counterpart was observed (Figures S1B and S1C; see Tables S1 and S2 for a listing of all K_D values measured in this study). In contrast, the PHD only bound the C-terminally labeled peptides irrespective of the modification status of K9, but not the

(D) Cellular lysates or recombinant proteins (top) were dialyzed against the indicated sources (bottom) and analyzed by histone peptide pull-down as in (B). (E) Fluorescence polarization experiment using purified recombinant 6×HIS-UHRF1 directly. H3 peptides were linked to fluorescein at the N terminus (FAM-H3[1–15]) via an amide bond.

(F) Fluorescence polarization experiment using purified recombinant 6×HIS-UHRF1 directly. A non-natural lysine at the C terminus was added and labeled with fluorescein at the ε-amino group (H3[1–15]-K[FAM]).

(G) Fluorescence polarization experiment using purified recombinant 6×HIS-UHRF1 after dialysis against HeLa NE. H3 peptides were linked to fluorescein at the N terminus (FAM-H3[1–15]) via an amide bond.

(H) Fluorescence polarization experiment using purified recombinant 6×HIS-UHRF1 after dialysis against HeLa NE. A non-natural lysine at the C terminus was added and labeled with fluorescein at the ε-amino group (H3[1–15]-K[FAM]). See also Figure S1 and Tables S1 and S2.

N-terminally labeled forms. Our findings provided an experimental approach to quantitatively define the interaction properties of UHRF1 and to dissect the contributions of the TTD and PHD within the full-length protein.

Since the observed H3 methylation-specific interaction of UHRF1 in the cell extract resembled that of the TTD, while the methylation nonspecific interaction of purified UHRF1 corresponded to that of the PHD, we reasoned that cellular cofactors direct differential binding modes relying on one or the other module. To test this, we set up a dialysis experiment, consecutively exposing recombinant 6×HIS-UHRF1 purified from *E.coli* to HeLa NE, but separated by a membrane with a very low (3 kDa) molecular weight cutoff (Figure 1C). After one round of dialysis, interaction with H3K9me0 was significantly decreased, while binding to H3K9me3 appeared unaffected (Figure 1D). After two rounds of dialysis, the interaction of the recombinant, dialyzed protein fully resembled that of the endogenous UHRF1 in HeLa NE. In parallel, the endogenous UHRF1 protein in the HeLa NE used for dialysis changed its properties, now binding H3K9me0 and H3K9me3 peptides equally well. Similar behavior was observed when NE from Sf9 insect cells instead of HeLa NE was used, indicating a general phenomenon (Figure S1D).

Quantitative FP measurements confirmed this switch in binding behavior. Purified, recombinant 6×HIS-UHRF1 did not bind N-terminally labeled H3K9me0 or H3K9me3 peptides (Figure 1E). Conversely, the protein interacted with C-terminally labeled H3 peptides with a slight preference for the K9me3 over the K9me0 state (Figure 1F). After two rounds of dialysis against HeLa NE, the properties changed completely. Interaction with H3K9me0 peptides irrespective of labeling at the N or C terminus was lost, while the H3K9me3 mark on both substrates was recognized, indicating that the TTD was responsible for the interaction and that any PHD binding contribution was removed (Figures 1G and 1H). We then performed consecutive dialysis experiments using UHRF1 with different tags (Figure 1D). Recombinant, bacterially expressed MBP-UHRF1, which bound equally well to H3K9me0 and H3K9me3 peptides, was dialyzed against 6×HIS-UHRF1 that had been already dialyzed twice against HeLa NE. Pull-down experiments showed that MBP-UHRF1 could be activated for specific H3K9me3 interaction using this scheme. Overall, the results indicated that small cofactors are transferred from HeLa NE to a recombinant protein, which can also be transferred to another recombinant protein.

Different H3 Tail Binding Modes of UHRF1 Are Mediated by the TTD and PHD Domains

We reasoned that the differential behavior of UHRF1 might be the consequence of allosteric regulation inducing conformational changes of the protein. Therefore, we compared the hydrodynamic properties of purified recombinant UHRF1 before and after dialysis against HeLa NE by analytical ultracentrifugation (Figure 2A). UHRF1 in a matched buffer control had a sedimentation coefficient around 3.7 S. The fit in the continuous c(s, ff0) model suggested that the majority of molecules displayed a frictional coefficient around 1.66 (Schuck and Rossmanith, 2000). After dialysis against HeLa NE, this distribution was significantly shifted toward lower frictional coefficients, demonstrating that the protein adopted a different overall conformation.

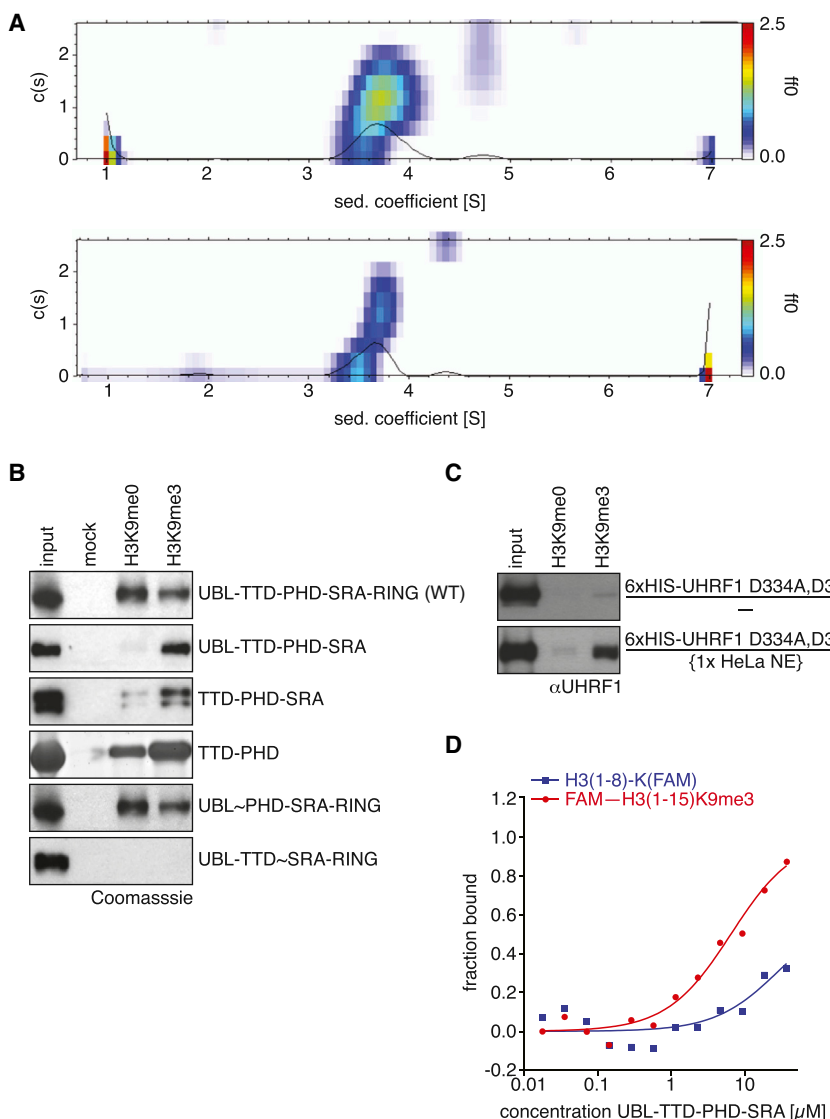
To gain further insights into the regulation of UHRF1, we analyzed a series of mutant recombinant proteins (Figure 2B). Deletion of the TTD had no effect on the interaction of UHRF1 with H3K9me0 and H3K9me3. Deletion of the PHD or mutagenesis of two key residues therein abolished H3 tail binding in pull-down (Figure 2C) and FP experiments (Figures S2A and S2B). The same mutations, however, had no effect on the interaction of the protein dialyzed against HeLa NE with H3K9me3. The results were consistent with the PHD mediating H3K9me0/H3K9me3 interaction in the form of the recombinant protein and the TTD mediating H3K9me3 binding after dialysis against HeLa NE. They also implied that the TTD is unavailable for histone binding in the state of the pure recombinant protein.

Deletion of the C-terminal region resulted in a recombinant UHRF1 protein that specifically recognized the H3K9me3 peptide in pull-down (Figure 2B) as well as FP (Figure 2D) experiments, reminiscent of the wild-type recombinant protein after HeLa NE dialysis. In this construct, the TTD is clearly available for binding the H3K9me3 tail. While a fragment containing only the TTD, PHD, and SRA domains showed similar preference for H3K9me3, the isolated TTD-PHD fragment displayed intermediate behavior. It bound to H3K9me3 and, somewhat weaker, to H3K9me0. FP analysis indicated that this fragment could interact with the C-terminally labeled H3K9me0 and H3K9me3 peptides and also with the N-terminally labeled H3K9me3 peptide, but not with the N-terminally labeled H3K9me0 peptide (Figure S2C). Binding to the C-terminally labeled peptides was overall stronger compared to the N-terminally labeled peptide, and there was a slight preference for the H3K9me3 over the H3K9me0 state. Recent work has suggested a cooperative mode of interaction involving simultaneous recognition of the extreme N terminus of H3 by the PHD and of the K9me3 mark by the TTD in this context (Arita et al., 2012; Cheng et al., 2013; Rothbart et al., 2013; Xie et al., 2012). However, since the full-length protein dialyzed against HeLa NE did not bind the C-terminally labeled H3K9me0 peptide (Figure 1H), meaning that the PHD is not contributing to H3 interaction, but showed binding to the N-terminally labeled H3K9me3 peptide similar to the TTD (Figure S2D), we deduced that the behavior of the isolated TTD-PHD could not explain the binding properties of the full-length protein.

A PBR Sequence in the C-Terminal Domain of UHRF1 Binds to a Peptide-Binding Groove on the Surface of the TTD

Because of the altered methylation specificity of the UHRF1 C-terminal deleted protein, we further investigated the role of this region in regulating H3 tail binding. In immunoprecipitation experiments, the isolated C terminus bound to the isolated TTD (Figure S3A), but not the PHD domains of UHRF1 (Figure S3B) or the FYVE domain of the Eea1 protein (Figure S3C), which belongs to the RING superfamily. Isothermal titration calorimetry deduced a binding strength of the isolated C terminus to the TTD of 4 μM (Figure S3D).

Additional mapping identified a short region within the pre-RING region of the C terminus that was sufficient for binding the TTD in pull-down experiments (Figure 3A). Due to its high content of basic amino acids, we termed this stretch a polybasic



region (PBR) (Figure 1A). Previous analyses of the cooperative binding mode of the UHRF1 TTD-PHD fragment have implicated the short linker region between these domains in directing the synergistic recognition of H3K9me3 (Arita et al., 2012; Cheng et al., 2013; Rothbart et al., 2013; Xie et al., 2012). A peptide binding groove on the isolated TTD was found to bind to H3 tail peptides with low μM affinity (Nady et al., 2011) as well as to the TTD-PHD linker with relatively weak affinity ($K_D > 100 \mu\text{M}$). Interestingly, the PBR, the TTD-PHD linker region, and the H3 tail all share an RKS sequence motif (Figure 3B). We measured the K_D for binding of the TTD to the PBR at 4 μM , which was much lower than that for the free TTD-PHD linker peptide (Figure 3C) (Rothbart et al., 2013).

In order to further characterize the intramolecular interaction, we performed a nuclear magnetic resonance (NMR) titration of increasing concentrations of the PBR peptide into ^{15}N -labeled TTD. We observed significant chemical shift changes indicative of an interaction in the micromolar range (Figure S3E). Chemical

Figure 2. The C Terminus Blocks UHRF1 H3K9me3 Interaction

(A) Recombinant 6xHIS-UHRF1 either dialyzed against buffer (top) or against HeLa NE (bottom) was analyzed by analytical ultracentrifugation. Distribution of sedimentation coefficient (S , x axis), concentration ($c[S]$; left y axis), and frictional ratio (f/f_0 ; right y axis; intensity of the corresponding sedimentation coefficient is indicated by superposition of the heatmap).

(B) Recombinant proteins were incubated with the specified biotinylated H3 (1–20) peptides immobilized on streptavidin magnetic beads. Recovered material was analyzed by western blot. Input, 2%.

(C) Mutant recombinant UHRF1 protein was either analyzed directly or after dialysis against HeLa NE by histone pull-down experiment as in (B).

(D) Recombinant UHRF1 lacking the C terminus was analyzed in fluorescence polarization binding experiments. See also Figure S2 and Tables S1 and S2.

shift changes larger than 0.094 ppm were concentrated around the groove formed at the interface between the two tudor domains (Figure S3F). This region was previously shown to bind the sequence N-terminal to the methylated lysine in the complex of the TTD with H3K9me3 (Nady et al., 2011). It also accommodates the linker in the crystal structure of the H3K9me3/TTD-PHD complex, thereby directing the cooperative binding mode engaging both modules (Arita et al., 2012; Cheng et al., 2013; Rothbart et al., 2013; Xie et al., 2012). We therefore refer to this region of the TTD as the peptide-binding groove (Figure 3D). Although the PBR can bind to the same TTD peptide-binding groove as

the histone H3 peptide and the TTD-PHD linker, the observed chemical shift perturbations were more extensive, involving extra surface residues such as K187, E193, L225, I211, and D275 (Figures 3D and S3F).

To better understand how the PBR interacts with the TTD, we performed docking calculations with HADDOCK, which uses NMR chemical shift changes to guide the simulations (de Vries et al., 2007; Dominguez et al., 2003). Two plausible models of the docked PBR were deduced. These differed in the direction of the bound PBR peptide (Figure 3E). Model 1 suggested an important contribution of PBR residues R649 and K650, while model 2 implicated residues K648 and R649 for binding to the TTD. Mutagenesis analysis of PBR peptides by FP indicated an essential contribution of R649 (Figure 3F). Mutagenesis of K648 had a stronger effect compared to mutagenesis of K650. In contrast, mutagenesis of residues K644 and K646 had no effect on the interaction. Similar results were obtained for the TTD-PHD fragment (Figure S3G). While we were not able to

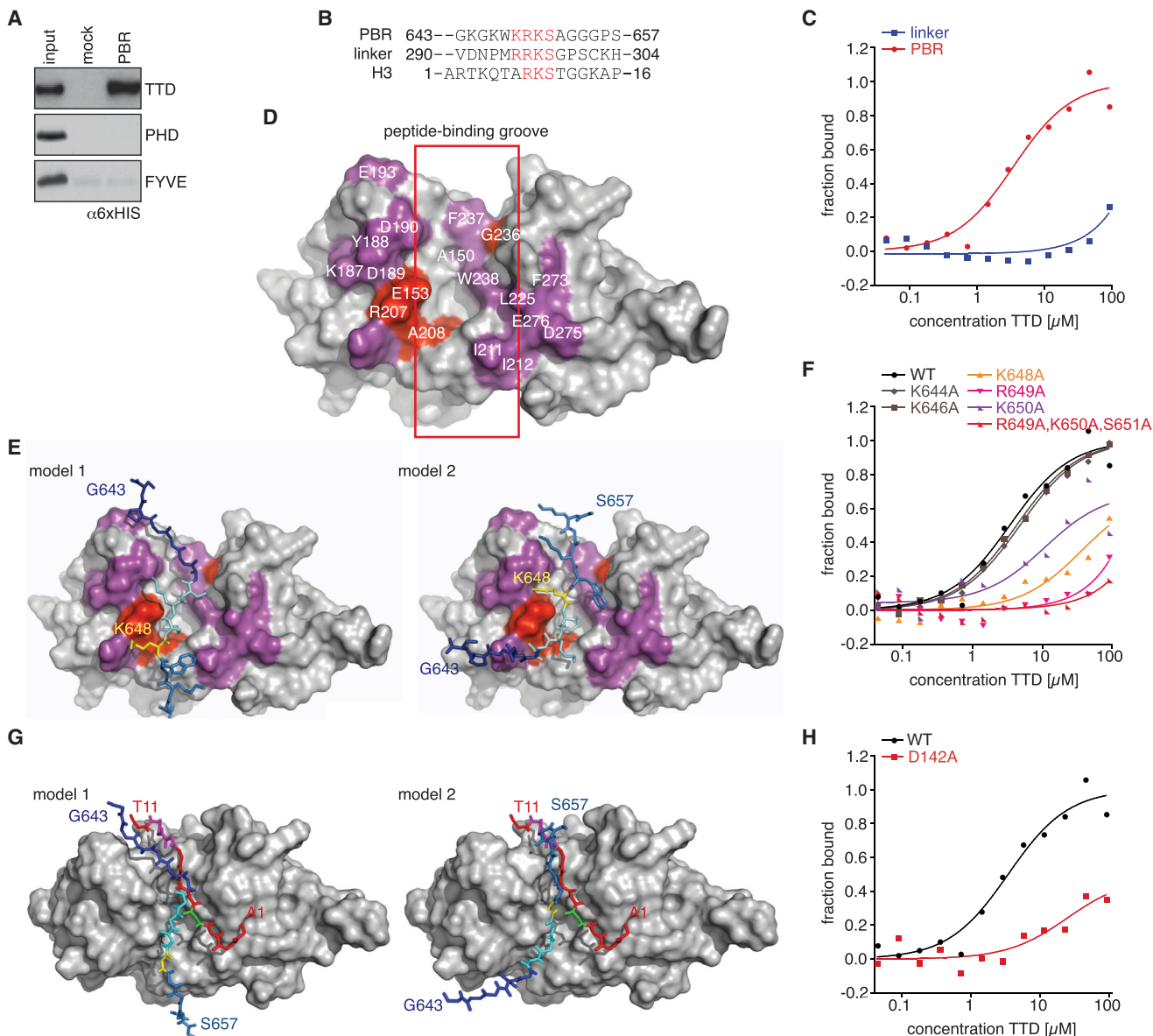


Figure 3. The PBR Sequence of the Pre-RING Region Binds a Peptide Groove on the Surface of the TTD

(A) TTD or PHD domains of UHRF1 or the FYVE domain of Eea1 were incubated with a biotinylated PBR peptide immobilized on streptavidin magnetic beads or beads alone (mock). Recovered material was analyzed by western blot. Input, 2%.

(B) Sequence comparison of the UHRF1 PBR and linker regions with the H3 tail.

(C) TTD of UHRF1 was analyzed in fluorescence polarization binding experiments with peptides corresponding to the UHRF1 linker or PBR (FAM at the N terminus).

(D) Surface model of the TTD (Protein Data Bank ID [PDB] 2L3R). Residues with chemical shift changes >0.094 ppm upon titration of the PBR peptide are shown in purple; those lining the TTD peptide-binding groove (red box), which have disappeared upon titration of the PBR peptide, are shown in red.

(E) HADDOCK models of likely positions of the PBR peptide in the TTD peptide-binding groove. K648 is highlighted in yellow as a visual guide of the orientation of the peptide; R649, K650, S651 is shown in cyan; the N and C termini of the peptide are shown in blue and dark blue, respectively. Color codes of residues showing major changes upon addition of the PBR peptide are as in (D).

(F) TTD of UHRF1 was analyzed in fluorescence polarization binding experiments with the indicated wild-type (WT) or mutant FAM-PBR peptides.

(G) Overlay of the positioning of the H3 tail (red; K4 residue in green, K9 residue in purple) as determined in the TTD/H3K9me3 complex (PDB 2L3R) and the PBR sequence in model 1 and model 2 (color code as in E). Images were generated by PyMOL.

(H) Wild-type (WT) or D142A mutant TTD of UHRF1 was analyzed in fluorescence polarization binding experiments with WT FAM-PBR peptide. See also Figure S3 and Tables S1 and S2.

unambiguously discriminate between the two binding modes for the TTD/PBR interaction, the mutagenesis results favored model 2. Comparison of the TTD/PBR complex with the TTD/H3K9me3 (Figure 3G) or the TTD/linker (Figure S3H) complexes indicated a mutually exclusive binding mode.

While methylated K9 of H3 within the RKS motif binds in a pocket formed in the TTD, the RKS sequence of the PBR does not interact in the same region. Instead, the UHRF1 PBR is centrally located in the TTD peptide-binding groove. Indeed, mutagenesis of two caging aromatic acid residues implicated in methyl-lysine binding in the TTD/H3K9me3 complex had only a very limited effect on TTD/PBR interaction (Figure S3I). In both NMR models, R649 engages in hydrogen bonding with D142, and mutagenesis of this residue significantly impaired binding of the PBR to the TTD (Figure 3H). In model 2, K648 engages in hydrogen bonding with D189 and D190. These are critical residues in the TTD peptide-binding groove that interact with R296 of the anchored TTD-PHD linker and with T6 of the histone H3K9me3 peptide, respectively (Arita et al., 2012; Nady et al., 2011). While mutagenesis of R295 and R296 of the linker within the TTD-PHD fragment had no effect on PBR interaction, it resulted in a slight increase in binding to free linker peptide (Figure S3J).

The PBR Sequence Is Sufficient for Blocking H3K9me3 Binding of the TTD

Next, we investigated the role of the C-terminal domain of UHRF1 in regulating H3K9me3 binding of the TTD. While the C terminus did not show specific interaction with H3K9me0 or H3K9me3 peptides (Figures S4A and S4B), it severely reduced recovery of the TTD on H3K9me3 beads when titrated into histone peptide pull-down experiments (Figure 4A). Likewise, the C-terminal domain of UHRF1, but not the FYVE domain of Eea1, blocked TTD/H3K9me3 interaction in FP experiments (Figure 4B). Similar results were obtained for the TTD-PHD, TTD-PHD-SRA, and UBL-TTD-PHD-SRA recombinant fragments of UHRF1 (Figures S4C–S4E).

Titration of H3K9me3, but not H3K9me0 peptide, into an immunoprecipitation of the C terminus resulted in significantly reduced recovery of the TTD (Figure 4C). These results were confirmed using only the PBR region of the C-terminal domain. In FP experiments, the PBR peptide blocked binding of the TTD to the H3K9me3 peptide (Figure 4D). Mutagenesis of the K644 and K646 residues that were not implicated in the binding of the PBR to the TTD peptide-binding groove had only a limited effect. While mutagenesis of the K650 residue somewhat reduced the blocking effect of the PBR peptide, changing the individual K648 or R649, or the combined R649, K650, and S651 sites, resulted in severe loss of blocking. Similar results were obtained for the TTD-PHD (Figure S4F).

Only the PBR, but not the much weaker binding linker peptide, blocked interaction of the TTD with H3K9me3 (Figure S4G). This effect was abrogated in the D142A mutant (Figure S4H). Moreover, the PBR peptide competed with the N-terminally labeled H3K9me3, but not the C-terminally labeled H3K9me3 or H3K9me0 peptides, for binding to the TTD-PHD (Figures S4I–S4K). The results supported the idea that binding of either the H3K9me3 or PBR peptides to the TTD are mutually exclusive

and independent of linker function as well as PHD binding to the extreme N terminus of H3. Presence of an H3K9me3 peptide compromised the interaction of the TTD (Figure 4E) or TTD-PHD (Figure S4L) with the PBR, while a H3K9me0 peptide had a much reduced effect.

Next, we designed multiple UHRF1 protein constructs with mutations in the PBR region. While mutagenesis of K650 had no effect, the R649A mutant showed increased binding to H3K9me3 in FP experiments (Figure 4F). This effect was stronger when, in addition, the K650 and S651 or the K644, K646, K648, K650, and S651 residues were also mutated. The same mutations had only little effect on the interaction of UHRF1 with an H3K9me0 peptide (Figure S4M). Similarly, we found that the UHRF1 K644A,K646A,K648A,R649A,K650A,S651A mutant protein had increased binding to H3K9me3 in pull-down experiments (Figure 4G). While the results potentially implied that there are additional interfaces between the TTD and C terminus, they supported a blocking effect of the PBR in the context of the full-length UHRF1 protein.

The PBR of UHRF1 Interacts with PI5P

To isolate the small cellular cofactor of UHRF1, we set up a chromatographic purification scheme (Figures S5A and S5B). Dialyzed, recombinant UHRF1 and the associated factors from the HeLa NE (all presumably <3 kDa) were separated by reversed-phase chromatography. Individual fractions were lyophilized and then tested for their ability to induce H3K9me3-specific binding of full-length recombinant UHRF1. The activating factor(s) could be separated by step-wise elution at 50% acetonitrile from a C8 column (Figure S5C). While it was possible to further refine the purification scheme and to combine different chromatography methods, several attempts to identify the activating factors by mass spectrometry failed.

In order to gain insights into the nature of the compounds from another direction, we defined the region of UHRF1 binding the NE factor(s). To this end, different domains of UHRF1 were subjected to dialysis against HeLa NE. Material eluting at 50% acetonitrile in our purification scheme was analyzed in histone tail pull-down experiments with recombinant UHRF1. The fragments of UHRF1 containing the C-terminal domain (WT, UBL-TTD~SRA-RING, C terminus), but not those without the C terminus (UBL-TTD~SRA, UBL-TTD-PHD~SRA), were able to recruit factor(s) that induced H3K9me3-specific binding (Figure 5A). Indeed, dialysis of the C terminus against HeLa NE relieved its inhibition of the interaction between the TTD and H3K9me3 (Figure 5B), while dialysis of the TTD itself had no effect (Figure 5C).

Upon a closer look at the PBR sequence within the C terminus, we realized that it contains a motif ($K/R-(X)_n = 3-7-K-X-K/R-K/R$) that had been implied in binding PIPs (Lewis et al., 2011). Indeed, treatment with phospholipase A2 (PLA2) that hydrolyzes PIPs abolished the capability of HeLa NE to activate H3K9me3-specific binding of recombinant UHRF1 (Figure 5D). We then tested recombinant UHRF1 for interaction with different PIPs, its precursors, and related compounds in standard lipid dot blot assays (Figures S5D and S5E). Similar to the PHD domain of ING1, UHRF1 bound PI5P in these assays (Bua and Binda, 2009).

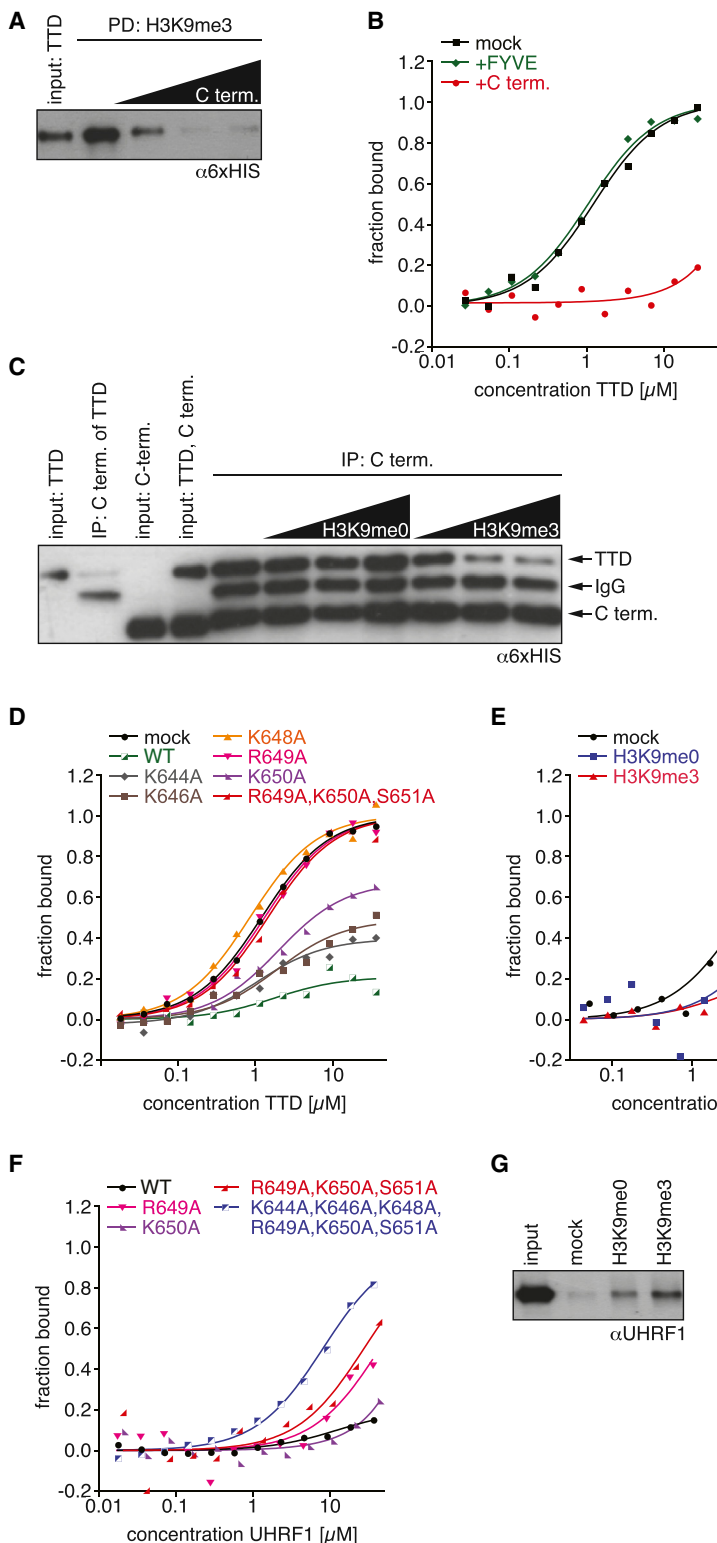


Figure 4. The PBR Blocks H3K9me3 Binding of the TTD

(A) TTD was incubated with increasing concentrations of the C terminus (molar ratio TTD:C term. = 2:1, 1:1, 1:1.5) and analyzed in pull-down (PD) experiments using an immobilized H3K9me3 peptide. Recovered material was analyzed by western blot. Input, 2%.

(B) TTD alone (mock) or in the presence of the C terminus of UHRF1 or the FYVE domain of Eea1 (1:2 molar ratio) was analyzed in fluorescence polarization binding experiments with FAM-H3(1–15)K9me3 peptide.

(C) C terminus was incubated with the TTD in the presence of increasing concentrations of the indicated H3(1–20) peptides (molar ratio TTD:C term.:peptide = 1:1:1, 1:1:2.5, 1:1:5, 1:1:7.5) and immunoprecipitated using antibodies against UHRF1. Recovered material was analyzed by western blot. Running positions of proteins recognized by the primary and/or secondary antibodies are indicated. Input, 5%.

(D) TTD alone (mock) or in the presence of the indicated PBR wild-type (WT) or mutant peptides (1:5 molar ratio) was analyzed in fluorescence polarization binding experiments with FAM-H3(1–15)K9me3 peptide.

(E) TTD alone (mock) or in the presence of the indicated H3(1–20) peptides (1:5 molar ratio) was analyzed in fluorescence polarization binding experiments with FAM-H3(1–15)K9me3 peptide.

(F) Wild-type (WT) UHRF1 or UHRF1 carrying the indicated mutations was analyzed in fluorescence polarization binding experiments with FAM-H3(1–15)K9me3 peptide.

(G) Mutant UHRF1 K644A,K646A,K648A,R649A, K650A,S651A was analyzed in a pull-down experiment using the specified biotinylated H3(1–20) peptides immobilized on streptavidin magnetic beads or beads alone (mock). Recovered material was analyzed by western blot. Input, 2%. See also Figure S4 and Tables S1 and S2.

As with ING1, additional interactions with other lipids (PI5P > PI3P = PA > PI3,5P₂ = PI4,5P₂ > PS) were also observed. As anticipated, no interaction of the H3K9me3-binding HP1 β protein with any of the lipids was seen.

We then used a liposome flotation assay to further define the PIP binding properties of UHRF1 (Figure 5E) (Rusten and Stenmark, 2006). As expected, the PHD domain of ING1 was only retained by liposomes containing PI5P, but not any of the other PIPs, while the FYVE domain of Eea1 was only retained on liposomes containing PI3P (Figures 5F and S5F) (Simonsen et al., 1998). Some background binding of both factors to PIP-free liposomes was also seen. While UHRF1 showed a similar background with PIP-free liposomes, it was only specifically retained on liposomes containing PI5P. No binding to liposomes containing PI3P, PI4P, PI3,5P₂, or PI4,5P₂ was observed.

Mapping of the interaction using lipid dot blots as well as liposome flotation assays defined the C terminus and, within that,

the PBR-containing pre-RING region as the PI5P binding domain of UHRF1 (Figures 5G, S5E, and S5F). Mutagenesis of R649, K650, and S651 within the PBR was sufficient to severely reduce binding of full-length UHRF1 as well as the pre-RING region to PI5P. Lastly, we compared binding of fluorescently labeled wild-type and R649A,K650A,S651A mutant PBR peptides to biotinylated PIPs immobilized on streptavidin beads (Figures 5H and S5G). A clear preference of the wild-type PBR for PI5P over PI, PI3P, PI4P, PI3,5P₂, and PI4,5P₂ was observed.

PI5P Regulates UHRF1 Interaction with the Modified or Unmodified H3 Tail

When titrated into immunoprecipitations of the C-terminal domain with the TTD, PI5P, but not PI4P, blocked the interaction (Figure 6A). Similarly, PI5P, but not PI4P, reduced the recovery of the TTD on the PBR peptide in pull-down experiments (Figure 6B).

We then asked whether PI5P could modulate H3 tail binding of UHRF1. In histone pull-down experiments, PI5P induced H3K9me3-specific binding of recombinant UHRF1 (Figure 6C). While PI3P also showed some activation, neither PA, PI, PI4P, PI3,5P₂, nor PI4,5P₂ had an effect. All attempts with PI5P containing different acyl chain lengths to induce H3K9me3-specific binding of UHRF1 in the FP-based experiments in solution failed. Also, the isolated inositolphosphate head groups of the PIPs had no effect (not shown).

To further investigate whether PI5P is indeed the cellular molecule regulating UHRF1, we made use of a specific kinase. PIP4K α transduces together with PIP4K β to the cell nucleus and phosphorylates PI5P on the 4-position, thereby yielding PI4,5P₂ (Bultsma et al., 2010). Addition of PIP4K α and ATP to an H3 tail pull-down reaction of recombinant UHRF1 abolished the activating function of PI5P (Figure S6). ATP alone had no effect, and the kinase did not alter the outcome with PI4P in this assay. We then incubated HeLa NE or a buffer control with PIP4K α and either ATP or the nonhydrolysable ATP γ S. UHRF1 was dialyzed against the treated lysate or buffer and analyzed in H3 tail pull-down experiments. Pretreatment of the HeLa NE with ATP and PIP4K α abolished the activating effect of the lysate (Figure 6D). Incubation of the HeLa NE with ATP alone or PIP4K α and ATP γ S also slightly induced some H3K9me3-specific binding of UHRF1. In contrast, pretreatment with ATP γ S had no effect. We think ATP and PIP kinase(s) present in the NE might account for these observations. No effect was observed with the buffer control, and there was no differential binding of the recombinant UHRF1 to H3K9me0 and H3K9me3. Altogether, the results indicated that PI5P is a cellular coactivator of UHRF1, allosterically regulating binding to different modification states of the H3 tail.

PI5P Directs TTD-Dependent UHRF1 Localization to Heterochromatin

Previous studies have found both strong and limited localization of UHRF1 to H3K9me3-enriched heterochromatin (Karagianni et al., 2008; Nady et al., 2011; Papait et al., 2007). We hypothesized that these discrepancies might be due to different cellular systems and conditions analyzed. We found that a large fraction (58%) of NIH 3T3 cells transiently expressing

mCherry-UHRF1 showed colocalization of the fusion protein with DAPI-dense and H3K9me3-positive foci of pericentromeric heterochromatin. Lower enrichment at these regions (intermediate) was seen for 29% of cells, while 13% of cells displayed diffuse nuclear distribution (Figure S7A). Mutation of two residues in the aromatic cage implicated in methyl-lysine binding in the TTD/H3K9me3 complex resulted in significantly more cells (64%) showing intermediate and diffuse phenotypes, while 36% of cells showed dotted UHRF1 Y188A,Y191A distribution (Figure S7B). The results suggested that other domains of the protein besides the TTD are also involved in heterochromatin localization. Indeed and in agreement with recent findings (Liu et al., 2013), after mutation of both the TTD and SRA domains, no heterochromatin localization of mCherry-UHRF1 was detected (Figure S7C). While the exact regulation of UHRF1 subnuclear and chromatin association is unclear, the protein might rely on different domains for target binding, and there could be a cell-cycle dependency (Papait et al., 2007).

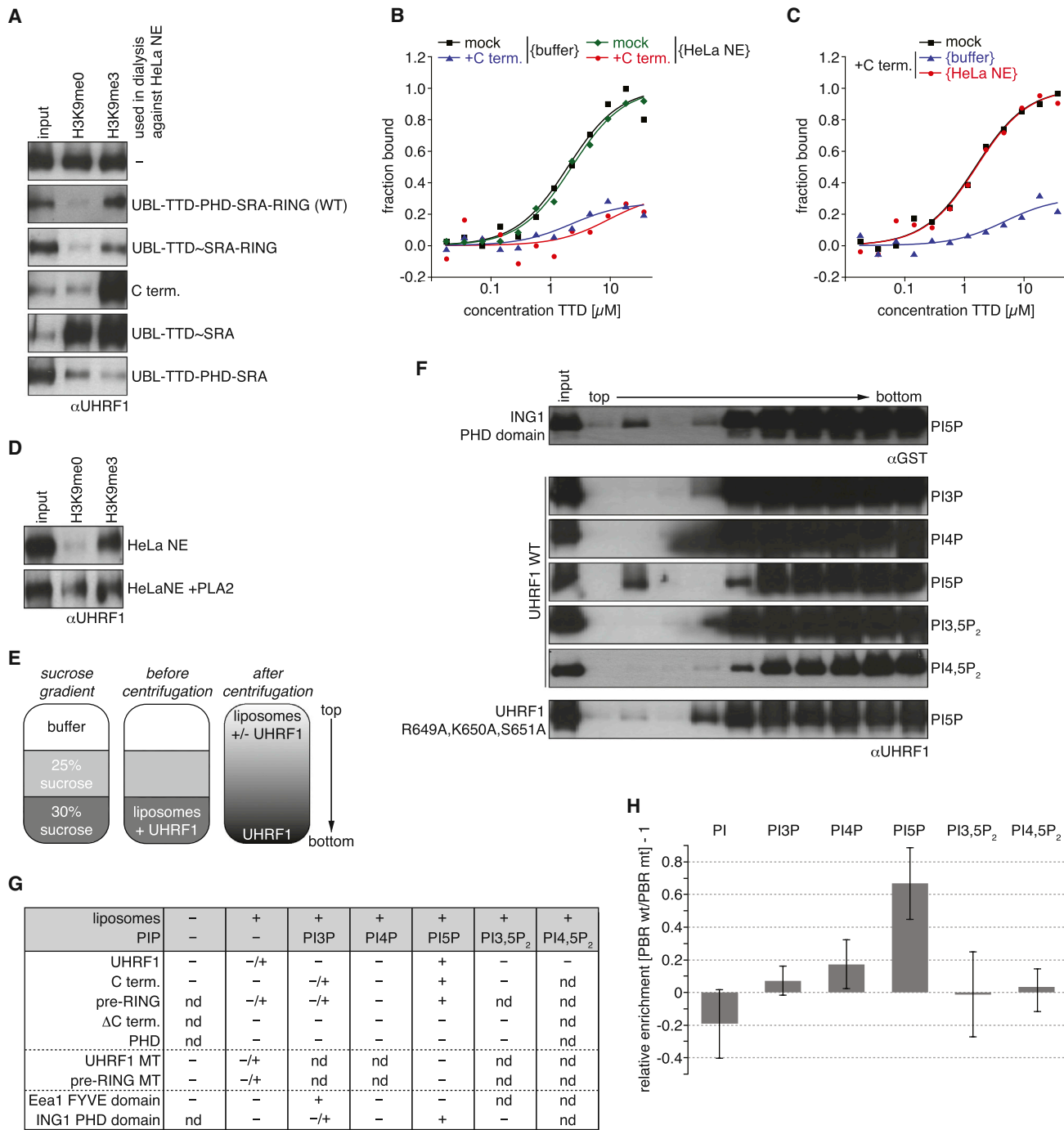
To determine the regulatory role of the PBR, we coexpressed GFP-tagged wild-type or mutant (K644A,K646A,K648A,R649A, K650A,S651A) pre-RING domain together with mCherry-UHRF1 in NIH 3T3 cells (Figures 7A and S7D). We thought this region might exert dual effects by simultaneously interfering with TTD/H3K9me3 binding as well as by titrating endogenous PI5P. Quantification of the different phenotypes indicated that an average of 12% of cells exhibited a shift in their mCherry-UHRF1 distribution from dotted to intermediate or diffuse appearance upon expression of wild-type GFP-pre-RING. This effect was not seen for coexpression of mCherry-UHRF1 with the mutant GFP-pre-RING (Figures 7B and S7E).

To further establish a regulatory role of PI5P for UHRF1, we made use of the PIP4K kinases to manipulate nuclear levels of the cofactor. Consistent with the phenotypes of pre-RING overexpression, coexpression with MYC-PIP4K α and PIP4K β (PIP4K WT) relative to coexpression of empty vector resulted in an average of 9% fewer cells displaying the nuclear dotted pattern of mCherry-UHRF1. In contrast, kinase mutant PIP4Ks (PIP4K α G131L,Y138F and PIP4K β D278A) had no such effect (Figures 7C and S7F–S7H). Given that only a fraction of cells in the population (on average 22%) relied on the TTD for localization to pericentric heterochromatin, we deduced from these experiments that PI5P binding to the PBR has a marked impact (~40%) on heterochromatin association of this UHRF1 subpopulation.

DISCUSSION

Regulation of UHRF1 H3 Tail Binding by Conformational Rearrangements Allosterically Induced by PI5P

By identifying a mode of regulation of UHRF1 by a cellular cofactor, our findings clarify discrepancies in the literature regarding the binding activities and domain usage of this important epigenetic regulator. Various reports used different experimental systems (i.e., protein expression in bacteria, which do not have PIPs, versus expression in insect cells, reticulocyte lysate, or mammalian cells, which all contain PIPs) and investigated full-length, deletion mutants, or point mutants of UHRF1 proteins. Distinct domains were implicated in binding to

**Figure 5. The PBR of UHRF1 Interacts with PI5P**

(A) The indicated fragments of UHRF1 were dialyzed against HeLa NE. Proteins and cellular factors inside the dialysis membrane were separated on a C8 reversed-phase column. Recombinant 6×HIS-UHRF1 was incubated with the material eluting at 50% acetonitrile and probed in a histone peptide pull-down experiment. Recovered material was analyzed by western blot. Input, 2%.

(B) TTD alone (mock) or incubated with the C terminus dialyzed against HeLa NE or buffer control (molar ratio TTD:C term. = 1:2) was analyzed in fluorescence polarization binding experiments using FAM-H3(1–15)K9me3 peptide.

(C) TTD was dialyzed against buffer or HeLa NE. Protein alone (mock) or in the presence of the C terminus was analyzed in fluorescence polarization binding experiments using FAM-H3(1–15)K9me3 peptide.

(legend continued on next page)

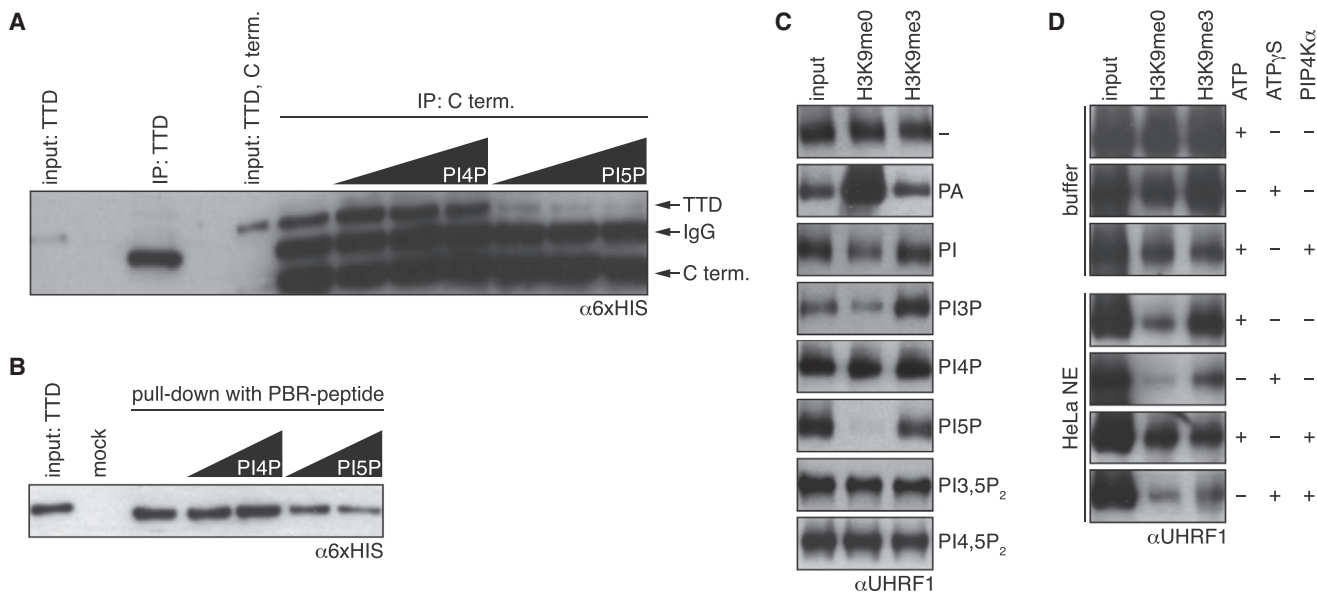


Figure 6. PI5P Releases Blocking of the TTD by the C Terminus

(A) C terminus was incubated with TTD in the presence of increasing concentrations of the indicated PIPs (molar ratio TTD:C term.:PIP = 1:1:5, 1:1:10, 1:1:20) and immunoprecipitated using antibodies against UHRF1. Recovered material was analyzed by western blot. Running positions of proteins recognized by the primary and/or secondary antibodies are indicated. Input, 5%.

(B) TTD was incubated with increasing concentrations of the indicated PIPs (molar ratio TTD:PIP = 1:5, 1:10) and analyzed in pull-down experiments using an immobilized PBR peptide. Recovered material was analyzed by western blot. Mock, pull-down with beads only; input, 2%.

(C) UHRF1 in the presence of the indicated lipids (2-fold molar excess) was incubated with the specified biotinylated H3(1–20) peptides immobilized on streptavidin magnetic beads. Recovered material was analyzed by western blot. Input, 2%.

(D) Recombinant UHRF1 was dialyzed against buffer or HeLa NE that was incubated with the indicated combinations of PIP4K α , ATP, or ATP γ S. After dialysis, the protein was probed in histone peptide pull-down reactions. Recovered material was analyzed by western blot. Input, 2%. See also Figure S6.

unmodified and K9me3 H3, and different interaction specificities were observed (Hu et al., 2011; Karagianni et al., 2008; Liu et al., 2013; Rajakumara et al., 2011; Rottach et al., 2010; Wang et al., 2011). We propose that most of the differences can be explained on the basis of the following regulatory mechanism. In the ground state of the recombinant protein or highly purified cellular protein, the C-terminal region of UHRF1 is folded back onto the middle region with the PBR sequence bound to the peptide-binding groove of the TTD (Figure 7D, top). This prevents the interaction of the TTD-PHD linker and also the H3 N-terminal tail with the TTD (Figure 4) (Nady et al., 2011). In this state, the PHD domain is able to bind to the extreme unmodified N terminus of H3. In an intermediate state that is artificially stabilized by mutagenesis of the PBR, the blockage of the TTD is released (Figure 7D, middle). We think this conformation of UHRF1 reflects the cooperative mode that we and others have observed

for the isolated TTD-PHD fragment (Arita et al., 2012; Cheng et al., 2013; Rothbart et al., 2013; Xie et al., 2012). It is characterized by a slight preference for H3K9me3 over the unmodified state, as seen for C-terminally labeled peptides (H3[1–15]-K [FAM]). Here, the linker sequence occupies the peptide-binding groove of the TTD. The N terminus of the H3 tail can bind to the PHD, while the aromatic cage of the TTD can recognize K9me3. In an activated state, the PBR is bound by PI5P, further stabilizing the domain orientation, giving TTD access to H3K9me3. Large conformational rearrangements not only free the TTD for H3K9me3 binding, but also block the PHD from binding the extreme unmodified N terminus of H3 (Figure 7D, bottom).

Further biophysical and structural studies will be needed to clarify the exact nature of the overall conformational rearrangements of the protein in the different states as well as the exact binding modes of the H3 tail and PI5P to UHRF1. The

- (D) Recombinant UHRF1 was dialyzed against untreated HeLa NE or HeLa NE that was incubated with phospholipase A2. After dialysis, the protein was probed in a histone peptide pull-down experiment. Recovered material was analyzed by western blot. Input, 2%.
- (E) Scheme of liposome flotation assay. The sucrose gradient was loaded with liposomes and UHRF1. After centrifugation, the gradient was fractionated and analyzed for localization of UHRF1.
- (F) The indicated proteins were incubated with liposomes containing the indicated PIPs. Fractions of the liposome flotation assay after centrifugation were analyzed by western blot. WT, wild-type; input, 5%.
- (G) Summary of multiple liposome flotation assays using different proteins. MT, mutation R649A,K650A,S651A. +, major protein signal at the top of the gradient; –/+, minor protein signal at the top of the gradient; nd, not determined.
- (H) Fluorescein-labeled wild-type (WT) or R649A,K650A,S651A mutant (MT) PBR peptides were incubated with the indicated biotinylated PIPs immobilized in 96-well plates. Fluorescence signals after washing were recorded. Averaged ratio of enrichment of WT versus MT of four independent experiments is plotted. Error bars correspond to error propagation of SEM reflected in five independent experiments. See also Figure S5 and Tables S1 and S2.

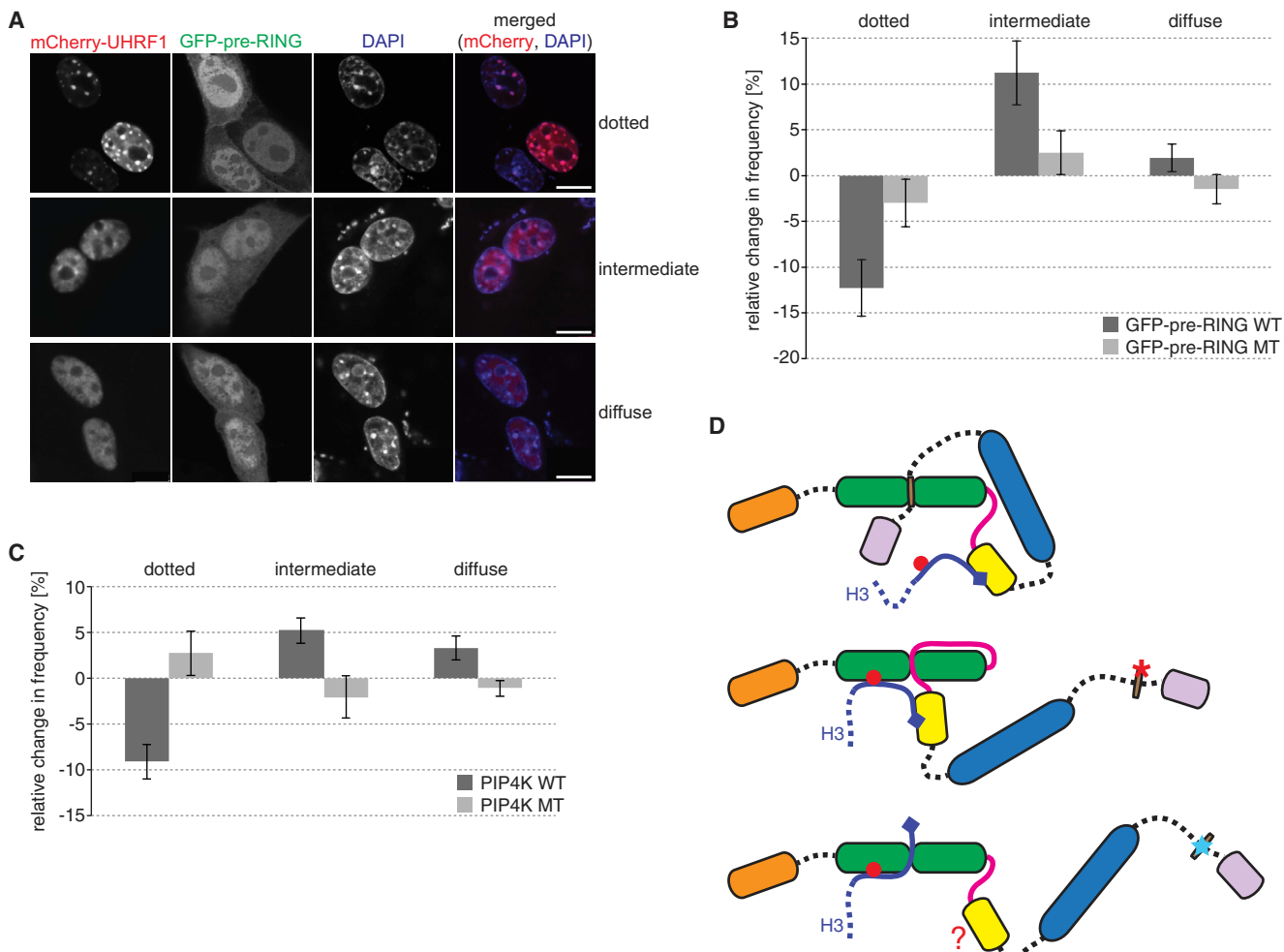


Figure 7. Nuclear PI5P Regulates Heterochromatin Association of UHRF1

(A) NIH 3T3 cells were transfected with mCherry-UHRF1 together with GFP-pre-RING. Fluorescence signals were analyzed by confocal microscopy. Images of representative cells of different phenotypes observed at the indicated frequencies ($n > 500$) are shown. DAPI was used to stain DNA. Scale bar, 10 μ m.

(B) Histogram showing changes in frequencies of observed nuclear distribution of mCherry-UHRF1 when coexpressing GFP-pre-RING wild-type (WT) or GFP-pre-RING K644A,K646A,K648A,R649A,K650A,S651A (MT) relative to coexpression of a GFP control in NIH 3T3 cells as classified in (A) ($n > 500$). Error bars represent error propagation of SEM reflected in four independent experiments.

(C) Histograms showing changes in frequencies of observed nuclear distribution of mCherry-UHRF1 coexpressing MYC-PIP4K α and untagged PIP4K β (PIP4K WT) or MYC-PIP4K α G131L,Y138F and untagged PIP4K β D278A (PIP4K MT) relative to coexpression of empty vector in NIH 3T3 cells as classified in (A) ($n > 500$). Error bars represent error propagation of SEM reflected in four independent experiments.

(D) Different conformational states of UHRF1. Top: the PHD mediates binding to unmodified extreme N terminus of H3 in the absence of PI5P, and the TTD is blocked from binding H3K9me3 by the PBR. Middle: when the PBR is mutated (red asterisk), it is dissociated from the TTD. The linker can mediate cooperative binding of the H3 tail by the PHD and TTD domains. Bottom: PI5P (blue star) binding by the PBR results in conformational rearrangement. The TTD is free to bind the H3K9me3 tail. Unknown mechanisms (indicated by the question mark) block the PHD from binding the unmodified extreme N terminus of H3. See also Figure S7.

mechanism of PHD blocking in the activated state is particularly unclear at this point. Our data question whether the cooperative state seen for the TTD-PHD exists in the context of the full-length protein. It might be an artificial state of an isolated fragment. The increase seen in H3K9me3 binding of TTD-PHD over TTD varies from 2-fold (this study; Arita et al., 2012) to 5-fold (Cheng et al., 2013; Rothbart et al., 2013), which might be due to different experimental conditions. In all cases and likely due to the flexible linkage of the TTD and PHD, it is not sufficient to account for the large binding differences for the unmodified and K9me3 H3 tail observed for cellular UHRF1.

Whether the slight preference for the K9me3 over the unmodified H3 peptide with C-terminal fluorescein (H3[1–15]-K[FAM]; Figure 1 and Table S1) reflects cooperativity of TTD and PHD in the ground state remains to be seen.

How are the hydrophobic acyl chains of PI5P bound to UHRF1 outside of a lipid membrane or micellar structure? While mutagenesis of the PBR is sufficient to abolish interaction in the lipid flotation assay (Figure 5F), we think that other regions of the C terminus and/or additional unknown components are involved in PI5P binding. First, in the liposome flotation assay, only the polar head groups of the PIPs are exposed; the hydrophobic

acyl chains are embedded in the lipid layer. Nevertheless, inositol 1,5-bisphosphate is not sufficient to induce allosteric activation of UHRF1. Second, while addition of PI5P to UHRF1 activates the protein in pull-down assays, it does not have this effect in solution FP assays (data not shown). We speculate that the phospholipid might get artificially enriched on the surface of the beads used in the pull-down assays. In the nuclear extract, PI5P is bound by UHRF1 and likely other factors that might work as “sinks” for the PIP. For sufficient transfer across the dialysis membrane, PI5P might need other small molecules (e.g., ions, peptides, RNA, etc.) that stabilize it in solution.

Cellular Regulation of UHRF1

While our findings identify a role for PI5P in modulating UHRF1 function, regulation of the protein in the cellular context is likely more complicated. Recent work had reported partially overlapping and redundant roles of the TTD and SRA domains in UHRF1 localization, where the two regions appear to mediate crosstalk between H3K9 methylation and DNA methylation at the level of DNA methylation maintenance (Liu et al., 2013). In contrast, another report suggested that cooperative interplay of the TTD and PHD is required for this function (Rothbart et al., 2013). The fact that the concentration of PI5P in the nuclei of murine erythroleukemia cells increases 20-fold during G1 phase but drops after S phase (Clarke et al., 2001) could indicate that switching between the unmodified H3-binding ground state and the activated H3K9me3-binding state of UHRF1 is required for differential localization of the protein during the cell cycle (Papait et al., 2007). Further work will need to clarify the precise crosstalk of the chromatin modification binding TTD, PHD, and SRA domains of UHRF1 under defined cellular conditions. Regulation of H3K9me3 and unmodified H3 tail interaction by PI5P also likely has an impact on UHRF1 binding to and targeting of its enzymatic partners such as G9a, DNMT1, and HDAC1.

Another level of regulation of UHRF1 is provided by post-translational modifications. Several proteomics studies have defined serine phosphorylation events within the linker and C-terminal region. Also, acetylation of two lysine residues within the SRA was found (Choudhary et al., 2009; Dephoure et al., 2008; Olsen et al., 2010; Rigbolt et al., 2011). While the functions of most modifications are unknown, phosphorylation by CDK1 at S639 is involved in degradation of the protein (Ma et al., 2012). Phosphorylation of S298 within the linker by PKA interferes with TTD-PHD cooperativity *in vitro* (Arita et al., 2012). Based on our mutagenesis studies of the PBR, we speculate that phosphorylation of S651 (S651ph) might have a regulatory role in PI5P binding and in modulating H3 interaction of UHRF1 (Rigbolt et al., 2011).

We predict that PI5P, as well as other nuclear PIPs, might have more general, so far unrecognized roles in directly regulating the chromatin binding activity of different proteins. Consistent with a role in signaling, the amounts of certain nuclear PIPs are increased in mammalian cells by physiological ligands or processes as well as by cellular stresses (Shah et al., 2013). This might directly impact gene regulation. In general, nuclear phospholipids undergo changes in abundance that match the transcriptional activity during the cell cycle (Fraschini et al., 1999). Defining further chromatin proteins that are directly regulated

by PIPs or other phospholipids might establish new paradigms of signal transduction in the cell nucleus.

EXPERIMENTAL PROCEDURES

Reagents

Detailed listing of plasmids, peptides, antibodies, and proteins can be found in the [Supplemental Information](#).

Dialysis of UHRF1

Nuclear extracts were prepared as described (Dignam et al., 1983). Protein concentration ranged from 10–15 mg/ml. Proteins (5 mg in 400 µl) were dialyzed against 10 ml HeLa NE or comparable buffer (in 50 ml tubes) overnight in dialysis cups (Pierce) with a 3,500 Da molecular weight cutoff at 4°C.

Pull-Downs, Immunofluorescence and Fluorescence Polarization, and Liposome Flotation Assay

Experiments were performed as previously described (Fischle et al., 2008; Rusten and Stenmark, 2006), with minor modifications as can be found in the [Supplemental Experimental Procedures](#).

Binding of PBR Peptides to PIP Beads

A 10 µl slurry of PIP beads (Echelon Biosciences) was incubated with 20 ng of fluorescein-labeled PBR peptide. After washing, samples were transferred to black 96-well plates (Corning), and fluorescence intensity (excitation at 485 nm, emission at 535 nm) was measured in a HIDEX Chameleon II plate reader. Results from three successive reads were averaged, and recovery of the peptides was normalized relative to the input.

NMR Spectroscopy

Chemical shift changes of the residues of the TTD upon titration of unlabeled linker peptide were mapped using prior available chemical shift assignments deposited in the Biological Magnetic Resonance Bank (BMRB) (Nady et al., 2011).

Molecular Docking

Docking of the PBR peptide to the TDD was performed using HADDOCK v2.1 software (de Vries et al., 2007; Dominguez et al., 2003).

SUPPLEMENTAL INFORMATION

Supplemental Information includes Supplemental Experimental Procedures, seven figures, and two tables and can be found with this article online at <http://dx.doi.org/10.1016/j.molcel.2014.04.004>.

ACKNOWLEDGMENTS

We thank members of the Fischle lab for invaluable comments and discussions. Katharina Rehn helped with peptide synthesis, Nadin Zimmermann with MS analysis of peptides, and Sven Johannsson with quantitative analysis of cellular phenotypes. We are thankful to Thomas Conrad for fermenter cell culture and Christer Ejsing (University of Southern Denmark) for PIP MS work. K.A.G. was supported by an EMBO long-term fellowship; K.H.-H. is supported by a Marie Curie Fellowship (IEF, FP7). This work was funded by the Max Planck Society (W.F.), the German Research Foundation (DFG grants FI 1513/2-1 to W.F. and SCHW 1163/3-1 to D.S.), Cancer Research UK (N.D.), and the Natural Sciences and Engineering Research Council of Canada (grant 372475-10 to C.H.A.). C.H.A. holds a Canada Research Chair in Structural Genomics. The SGC is a registered charity (number 1097737) that receives funds from AbbVie, Boehringer Ingelheim, the Canada Foundation for Innovation, the Canadian Institutes for Health Research, Genome Canada through the Ontario Genomics Institute [OGL-055], GlaxoSmithKline, Janssen, Lilly Canada, the Novartis Research Foundation, the Ontario Ministry Research and Innovation, Pfizer, Takeda, and the Wellcome Trust (092809/Z/10/Z).

Received: February 5, 2014
Revised: March 11, 2014
Accepted: April 2, 2014
Published: May 8, 2014

REFERENCES

- Arita, K., Isogai, S., Oda, T., Unoki, M., Sugita, K., Sekiyama, N., Kuwata, K., Hamamoto, R., Tochio, H., Sato, M., et al. (2012). Recognition of modification status on a histone H3 tail by linked histone reader modules of the epigenetic regulator UHRF1. *Proc. Natl. Acad. Sci. USA* 109, 12950–12955.
- Barlow, C.A., Laishram, R.S., and Anderson, R.A. (2010). Nuclear phosphoinositides: a signaling enigma wrapped in a compartmental conundrum. *Trends Cell Biol.* 20, 25–35.
- Berkurek, A.C., Suetake, I., Arita, K., Takeshita, K., Nakagawa, A., Shirakawa, M., and Tajima, S. (2014). The DNA methyltransferase Dnmt1 directly interacts with the SET and RING finger-associated (SRA) domain of the multifunctional protein Uhrf1 to facilitate accession of the catalytic center to hemi-methylated DNA. *J. Biol. Chem.* 289, 379–386.
- Bostick, M., Kim, J.K., Estève, P.O., Clark, A., Pradhan, S., and Jacobsen, S.E. (2007). UHRF1 plays a role in maintaining DNA methylation in mammalian cells. *Science* 317, 1760–1764.
- Bronner, C., Fuhrmann, G., Chédin, F.L., Macaluso, M., and Dhe-Paganon, S. (2010). UHRF1 Links the Histone code and DNA Methylation to ensure Faithful Epigenetic Memory Inheritance. *Genet Epigenet* 2009, 29–36.
- Bua, D.J., and Bindra, O. (2009). The return of the INGs, histone mark sensors and phospholipid signaling effectors. *Curr. Drug Targets* 10, 418–431.
- Bua, D.J., Martin, G.M., Bindra, O., and Gozani, O. (2013). Nuclear phosphatidylinositol-5-phosphate regulates ING2 stability at discrete chromatin targets in response to DNA damage. *Sci Rep* 3, 2137.
- Bultsma, Y., Keune, W.J., and Divecha, N. (2010). PIP4Kbeta interacts with and modulates nuclear localization of the high-activity PtdIns5P-4-kinase isoform PIP4Kalpha. *Biochem. J.* 430, 223–235.
- Burgio, G., Onorati, M.C., and Corona, D.F. (2010). Chromatin remodeling regulation by small molecules and metabolites. *Biochim. Biophys. Acta* 1799, 671–680.
- Catimel, B., Yin, M.X., Schieber, C., Condron, M., Patsiouras, H., Catimel, J., Robinson, D.E., Wong, L.S., Nice, E.C., Holmes, A.B., and Burgess, A.W. (2009). PI(3,4,5)P3 Interactome. *J. Proteome Res.* 8, 3712–3726.
- Cheng, J., Yang, Y., Fang, J., Xiao, J., Zhu, T., Chen, F., Wang, P., Li, Z., Yang, H., and Xu, Y. (2013). Structural insight into coordinated recognition of trimethylated histone H3 lysine 9 (H3K9me3) by the plant homeodomain (PHD) and tandem tudor domain (TTD) of UHRF1 (ubiquitin-like, containing PHD and RING finger domains, 1) protein. *J. Biol. Chem.* 288, 1329–1339.
- Choudhary, C., Kumar, C., Gnad, F., Nielsen, M.L., Rehman, M., Walther, T.C., Olsen, J.V., and Mann, M. (2009). Lysine acetylation targets protein complexes and co-regulates major cellular functions. *Science* 325, 834–840.
- Clarke, J.H., Letcher, A.J., D'santos, C.S., Halstead, J.R., Jr., Irvine, R.F., and Divecha, N. (2001). Inositol lipids are regulated during cell cycle progression in the nuclei of murine erythroleukaemia cells. *Biochem. J.* 357, 905–910.
- de Vries, S.J., van Dijk, A.D., Krzeminski, M., van Dijk, M., Thureau, A., Hsu, V., Wassenaar, T., and Bonvin, A.M. (2007). HADDOCK versus HADDOCK: new features and performance of HADDOCK2.0 on the CAPRI targets. *Proteins* 69, 726–733.
- Dephoure, N., Zhou, C., Villén, J., Beausoleil, S.A., Bakalarski, C.E., Elledge, S.J., and Gygi, S.P. (2008). A quantitative atlas of mitotic phosphorylation. *Proc. Natl. Acad. Sci. USA* 105, 10762–10767.
- Dignam, J.D., Lebovitz, R.M., and Roeder, R.G. (1983). Accurate transcription initiation by RNA polymerase II in a soluble extract from isolated mammalian nuclei. *Nucleic Acids Res.* 11, 1475–1489.
- Dominguez, C., Boelens, R., and Bonvin, A.M. (2003). HADDOCK: a protein-protein docking approach based on biochemical or biophysical information. *J. Am. Chem. Soc.* 125, 1731–1737.
- Fischle, W. (2012). One, two, three: how histone methylation is read. *Epigenomics* 4, 641–653.
- Fischle, W., Franz, H., Jacobs, S.A., Allis, C.D., and Khorasanizadeh, S. (2008). Specificity of the chromodomain Y chromosome family of chromodomains for lysine-methylated ARK(S/T) motifs. *J. Biol. Chem.* 283, 19626–19635.
- Fiume, R., Keune, W.J., Faenza, I., Bultsma, Y., Ramazzotti, G., Jones, D.R., Martelli, A.M., Sommer, L., Follo, M.Y., Divecha, N., and Cocco, L. (2012). Nuclear phosphoinositides: location, regulation and function. *Subcell. Biochem.* 59, 335–361.
- Fraschini, A., Biggiogera, M., Bottone, M.G., and Martin, T.E. (1999). Nuclear phospholipids in human lymphocytes activated by phytohemagglutinin. *Eur. J. Cell Biol.* 78, 416–423.
- Gozani, O., Karuman, P., Jones, D.R., Ivanov, D., Cha, J., Lugovskoy, A.A., Baird, C.L., Zhu, H., Field, S.J., Lessnick, S.L., et al. (2003). The PHD finger of the chromatin-associated protein ING2 functions as a nuclear phosphoinositide receptor. *Cell* 114, 99–111.
- Hu, L., Li, Z., Wang, P., Lin, Y., and Xu, Y. (2011). Crystal structure of PHD domain of UHRF1 and insights into recognition of unmodified histone H3 arginine residue 2. *Cell Res.* 21, 1374–1378.
- Jones, D.R., Bultsma, Y., Keune, W.J., Halstead, J.R., Elouarrat, D., Mohammed, S., Heck, A.J., D'Santos, C.S., and Divecha, N. (2006). Nuclear PtdIns5P as a transducer of stress signaling: an in vivo role for PIP4Kbeta. *Mol. Cell* 23, 685–695.
- Karagianni, P., Amazit, L., Qin, J., and Wong, J. (2008). ICBP90, a novel methyl K9 H3 binding protein linking protein ubiquitination with heterochromatin formation. *Mol. Cell. Biol.* 28, 705–717.
- Lallous, N., Legrand, P., McEwen, A.G., Ramón-Maiques, S., Samama, J.P., and Birck, C. (2011). The PHD finger of human UHRF1 reveals a new subgroup of unmethylated histone H3 tail readers. *PLoS ONE* 6, e27599.
- Lewis, A.E., Sommer, L., Arntzen, M.O., Strahm, Y., Morrice, N.A., Divecha, N., and D'Santos, C.S. (2011). Identification of nuclear phosphatidylinositol 4,5-bisphosphate-interacting proteins by neomycin extraction. *Mol. Cell. Proteomics* 10, 003376.
- Liu, X., Gao, Q., Li, P., Zhao, Q., Zhang, J., Li, J., Koseki, H., and Wong, J. (2013). UHRF1 targets DNMT1 for DNA methylation through cooperative binding of hemi-methylated DNA and methylated H3K9. *Nat Commun* 4, 1563.
- Lu, C., and Thompson, C.B. (2012). Metabolic regulation of epigenetics. *Cell Metab.* 16, 9–17.
- Ma, H., Chen, H., Guo, X., Wang, Z., Sowa, M.E., Zheng, L., Hu, S., Zeng, P., Guo, R., Diao, J., et al. (2012). M phase phosphorylation of the epigenetic regulator UHRF1 regulates its physical association with the deubiquitylase USP7 and stability. *Proc. Natl. Acad. Sci. USA* 109, 4828–4833.
- Manzoli, F.A., Cocco, L., Facchini, A., Casali, A.M., Maraldi, N.M., and Grossi, C.E. (1976). Phospholipids bound to acidic nuclear proteins in human B and T lymphocytes. *Mol. Cell. Biochem.* 12, 67–71.
- Maraldi, N.M., Capitani, S., Caramelli, E., Cocco, L., Barnabei, O., and Manzoli, F.A. (1984). Conformational changes of nuclear chromatin related to phospholipid induced modifications of the template availability. *Adv. Enzyme Regul.* 22, 447–464.
- Nady, N., Lemak, A., Walker, J.R., Avvakumov, G.V., Karetta, M.S., Achour, M., Xue, S., Duan, S., Allali-Hassani, A., Zuo, X., et al. (2011). Recognition of multivalent histone states associated with heterochromatin by UHRF1 protein. *J. Biol. Chem.* 286, 24300–24311.
- Ndamukong, I., Jones, D.R., Lapko, H., Divecha, N., and Avramova, Z. (2010). Phosphatidylinositol 5-phosphate links dehydration stress to the activity of ARABIDOPSIS TRITHORAX-LIKE factor ATX1. *PLoS ONE* 5, e13396.
- Nishiyama, A., Yamaguchi, L., Sharif, J., Johmura, Y., Kawamura, T., Nakanishi, K., Shimamura, S., Arita, K., Kodama, T., Ishikawa, F., et al. (2013). Uhrf1-dependent H3K23 ubiquitylation couples maintenance DNA methylation and replication. *Nature* 502, 249–253.

- Olsen, J.V., Vermeulen, M., Santamaria, A., Kumar, C., Miller, M.L., Jensen, L.J., Gnad, F., Cox, J., Jensen, T.S., Nigg, E.A., et al. (2010). Quantitative phosphoproteomics reveals widespread full phosphorylation site occupancy during mitosis. *Sci. Signal.* 3, ra3.
- Papait, R., Pistore, C., Negri, D., Pecoraro, D., Cantarini, L., and Bonapace, I.M. (2007). Np95 is implicated in pericentromeric heterochromatin replication and in major satellite silencing. *Mol. Biol. Cell* 18, 1098–1106.
- Pasquali, C., Bertschy-Meier, D., Chabert, C., Curchod, M.L., Arod, C., Booth, R., Mechtlar, K., Vilbois, F., Xenarios, I., Ferguson, C.G., et al. (2007). A chemical proteomics approach to phosphatidylinositol 3-kinase signaling in macrophages. *Mol. Cell. Proteomics* 6, 1829–1841.
- Patel, D.J., and Wang, Z. (2013). Readout of epigenetic modifications. *Annu. Rev. Biochem.* 82, 81–118.
- Rajakumara, E., Wang, Z., Ma, H., Hu, L., Chen, H., Lin, Y., Guo, R., Wu, F., Li, H., Lan, F., et al. (2011). PHD finger recognition of unmodified histone H3R2 links UHRF1 to regulation of euchromatic gene expression. *Mol. Cell* 43, 275–284.
- Rigbolt, K.T., Prokhorova, T.A., Akimov, V., Henningsen, J., Johansen, P.T., Kratchmarova, I., Kassem, M., Mann, M., Olsen, J.V., and Blagoev, B. (2011). System-wide temporal characterization of the proteome and phosphoproteome of human embryonic stem cell differentiation. *Sci. Signal.* 4, rs3.
- Rose, H.G., and Frenster, J.H. (1965). Composition and metabolism of lipids within repressed and active chromatin of interphase lymphocytes. *Biochim. Biophys. Acta* 106, 577–591.
- Rothbart, S.B., Dickson, B.M., Ong, M.S., Krajewski, K., Houliston, S., Kireev, D.B., Arrowsmith, C.H., and Strahl, B.D. (2013). Multivalent histone engagement by the linked tandem Tudor and PHD domains of UHRF1 is required for the epigenetic inheritance of DNA methylation. *Genes Dev.* 27, 1288–1298.
- Rottach, A., Frauer, C., Pichler, G., Bonapace, I.M., Spada, F., and Leonhardt, H. (2010). The multi-domain protein Np95 connects DNA methylation and histone modification. *Nucleic Acids Res.* 38, 1796–1804.
- Rusten, T.E., and Stenmark, H. (2006). Analyzing phosphoinositides and their interacting proteins. *Nat. Methods* 3, 251–258.
- Schuck, P., and Rossmanith, P. (2000). Determination of the sedimentation coefficient distribution by least-squares boundary modeling. *Biopolymers* 54, 328–341.
- Shah, Z.H., Jones, D.R., Sommer, L., Foulger, R., Bultsma, Y., D'Santos, C., and Divecha, N. (2013). Nuclear phosphoinositides and their impact on nuclear functions. *FEBS J.* 280, 6295–6310.
- Sharif, J., and Koseki, H. (2011). Recruitment of Dnmt1 roles of the SRA protein Np95 (Uhrf1) and other factors. *Prog. Mol. Biol. Transl. Sci.* 101, 289–310.
- Sharif, J., Muto, M., Takebayashi, S., Suetake, I., Iwamatsu, A., Endo, T.A., Shinga, J., Mizutani-Koseki, Y., Toyoda, T., Okamura, K., et al. (2007). The SRA protein Np95 mediates epigenetic inheritance by recruiting Dnmt1 to methylated DNA. *Nature* 450, 908–912.
- Simonsen, A., Lippé, R., Christoforidis, S., Gaullier, J.M., Brech, A., Callaghan, J., Toh, B.H., Murphy, C., Zerial, M., and Stenmark, H. (1998). EEA1 links PI(3)K function to Rab5 regulation of endosome fusion. *Nature* 394, 494–498.
- Wang, C., Shen, J., Yang, Z., Chen, P., Zhao, B., Hu, W., Lan, W., Tong, X., Wu, H., Li, G., and Cao, C. (2011). Structural basis for site-specific reading of unmodified R2 of histone H3 tail by UHRF1 PHD finger. *Cell Res.* 21, 1379–1382.
- Wang, F., Yang, Y.Z., Shi, C.Z., Zhang, P., Moyer, M.P., Zhang, H.Z., Zou, Y., and Qin, H.L. (2012). UHRF1 promotes cell growth and metastasis through repression of p16(ink4a) in colorectal cancer. *Ann. Surg. Oncol.* 19, 2753–2762.
- Xie, S., Jakoncic, J., and Qian, C. (2012). UHRF1 double tudor domain and the adjacent PHD finger act together to recognize K9me3-containing histone H3 tail. *J. Mol. Biol.* 415, 318–328.

Molecular Cell, Volume 54

Supplemental Information

Accessibility of Different Histone H3-Binding Domains of UHRF1 Is Allosterically Regulated by Phosphatidylinositol 5-Phosphate

Kathy A. Gelato, Maria Tauber, Michelle S. Ong, Stefan Winter, Kyoko Hiragami-Hamada, Julia Sindlinger, Alexander Lemak, Yvette Bultsma, Scott Houlston, Dirk Schwarzer, Nullin Divecha, Cheryl H. Arrowsmith, and Wolfgang Fischle

SUPPLEMENTAL FIGURES

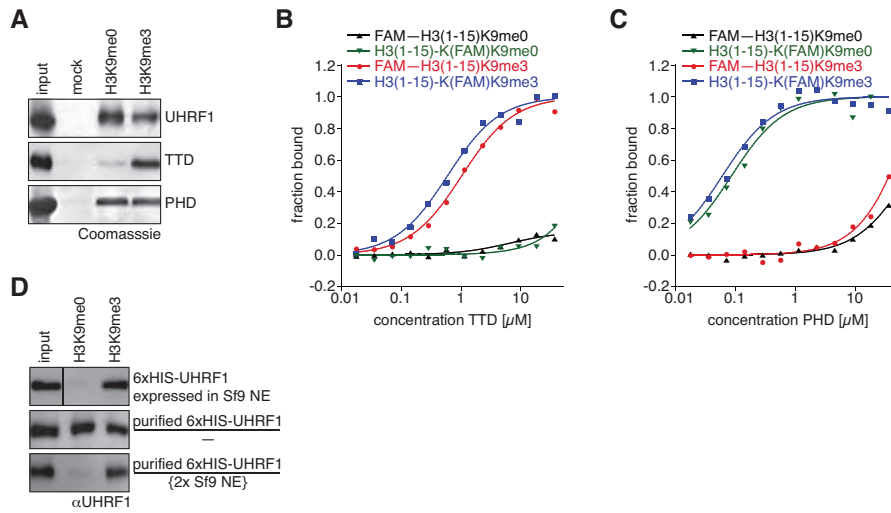


Figure S1. Different Functional States of the TTD and PHD Domains of UHRF1

Related to Figure 1

(A) UHRF1 or the isolated TTD or PHD domain were incubated with the specified biotinylated H3(1-20) peptides immobilized on streptavidin magnetic beads. Mock represents pull-down with beads only. Recovered material was analyzed by Coomassie staining. Input, 2%.

(B) and (C) Fluorescence polarization binding experiments of the TTD (B) or PHD (C) domain of UHRF1 using H3 peptides carrying the specified modification status on lysine 9 (K9). H3 peptides were either linked to fluorescein at the N terminus (FAM–H3[1-15]) via an amide bond or a non-natural lysine at the C terminus was added and labeled with amide-linked fluorescein at the ϵ -amino group (H3[1-15]-K[FAM]).

(D) Pull-down reactions using the indicated H3 peptides were performed using extracts from Sf9 cells expressing 6xHIS-UHRF1, 6xHIS-UHRF1 purified from this source after dialysis against buffer (–) or Sf9 cell nuclear extract (NE). Recovered material was analyzed by western blot. Input, 2%.

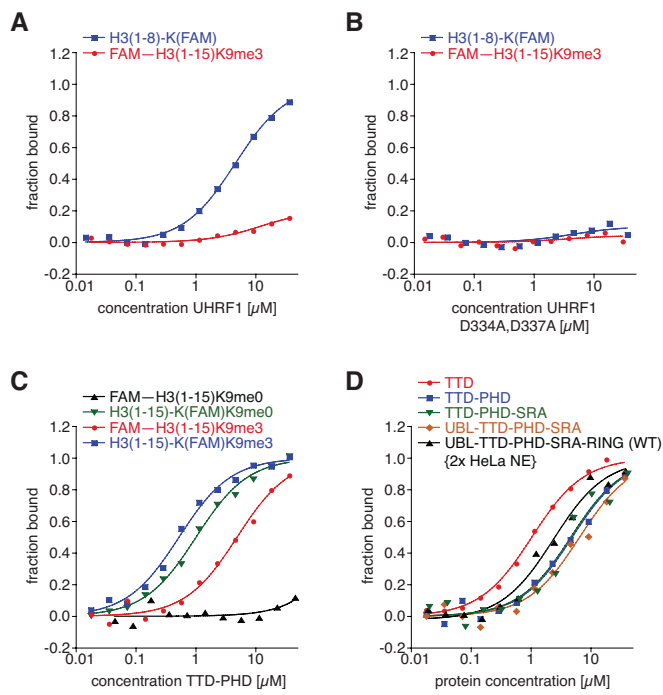


Figure S2. Fluorescence Polarization Binding Experiments of Different UHRF1 Wild-Type and Mutant Proteins

Related to Figure 2

(A)-(C) The specified proteins were analyzed in fluorescence polarization binding experiments using the indicated fluorescein-labeled peptides.

(D) The indicated recombinant protein fragments of UHRF1 or the wild-type (WT, UBL-TTD-PHD-SRA-RING) protein dialyzed twice against HeLa NE were analyzed in fluorescence polarization binding experiments using a FAM-H3(1-15)K9me3 peptide.

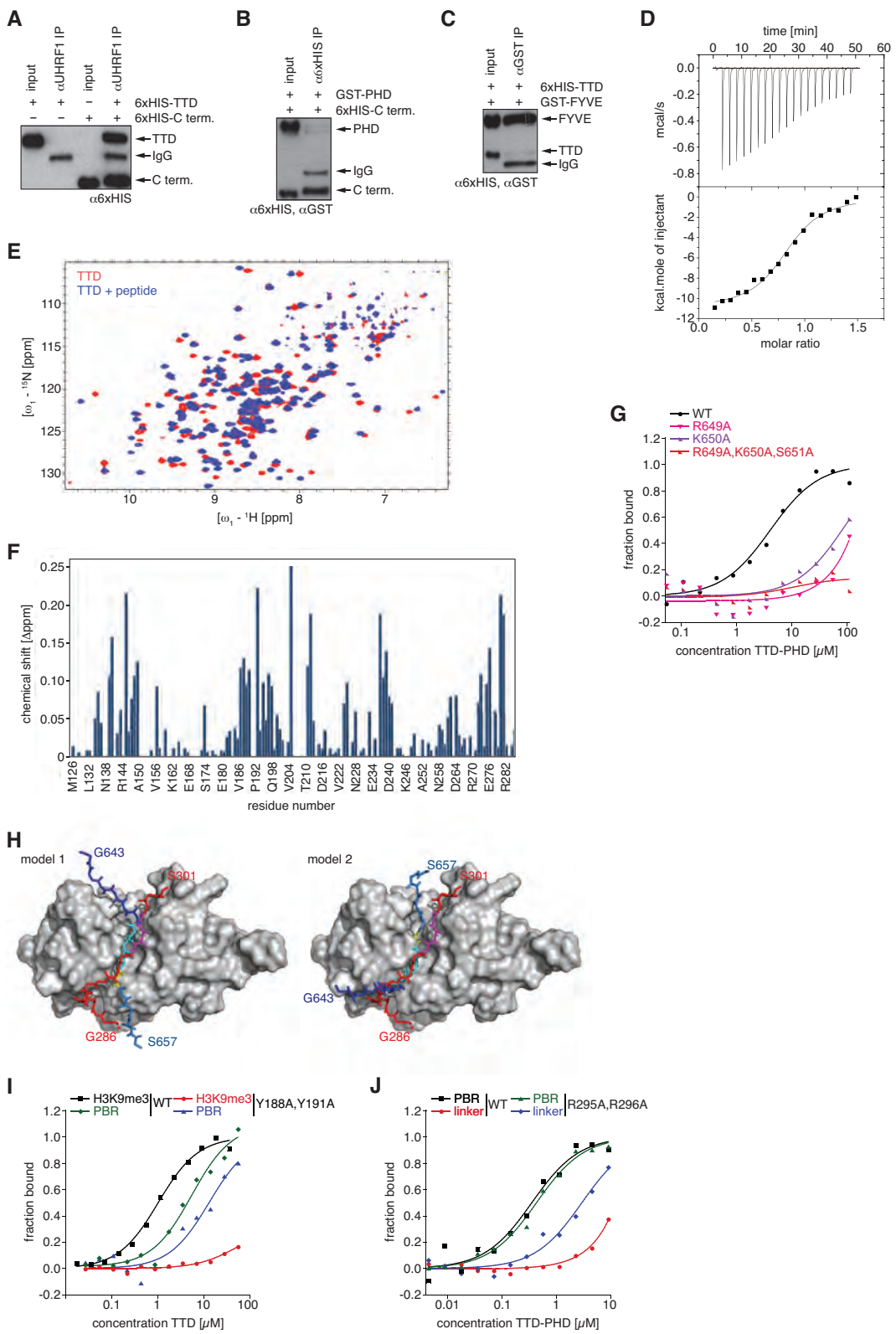


Figure S3. A PBR Region within the C Terminus of UHRF1 Interacts with the TTD

Related to Figure 3

(A)-(C) Immunoprecipitation experiments of the indicated recombinant protein domains. The 6xHIS-C terminus of UHRF1 was recovered by anti-UHRF1 antibodies in presence of 6xHIS-TTD (A) or GST-PHD (B). (C) The GST-tagged FYVE domain of Eea1 was precipitated by anti-GST antibodies in presence of 6xHIS-TTD of UHRF1. Recovered material was analyzed by western blot. Running positions of proteins recognized by the primary and/or secondary antibodies are indicated. Input, 5%.

(D) Interaction of the TTD with the C terminus was analyzed by isothermal titration calorimetry. A representative titration is shown.

(E) HSQC spectra showing overlay of signals of ^{15}N -TTD in absence and presence of PBR peptide at 1:10 molar ratio.

(F) Histogram showing chemical shift changes of the ^{15}N -TTD upon titration with the PBR peptide at a 1:10 molar ratio.

(G) The TTD-PHD fragment of UHRF1 was analyzed in fluorescence polarization binding experiments using fluorescein-labeled wild-type (WT) or mutant PBR peptides.

(H) Overlay of the positioning of the TTD-PHD linker (red, R295 and R296 residues in purple) as determined in the TTD-PHD/H3K9me3 complex (pdb: 3ASK) and the PBR sequence in model 1 and model 2 (color code as in figure 3E). Images were generated by PyMol.

(I) Wild-type TTD domain or TTD domain mutated in the aromatic cage residues Y188 and Y191 was analyzed in fluorescence polarization binding experiments using FAM-H3(1-15)K9me3 or FAM-PBR peptides.

(J) Wild-type TTD-PHD domain (WT) or TTD-PHD domain mutated in the linker residues R295 and R296 (MT) was analyzed in fluorescence polarization binding experiments using FAM-H3(1-15)K9me3 or FAM-PBR peptides.

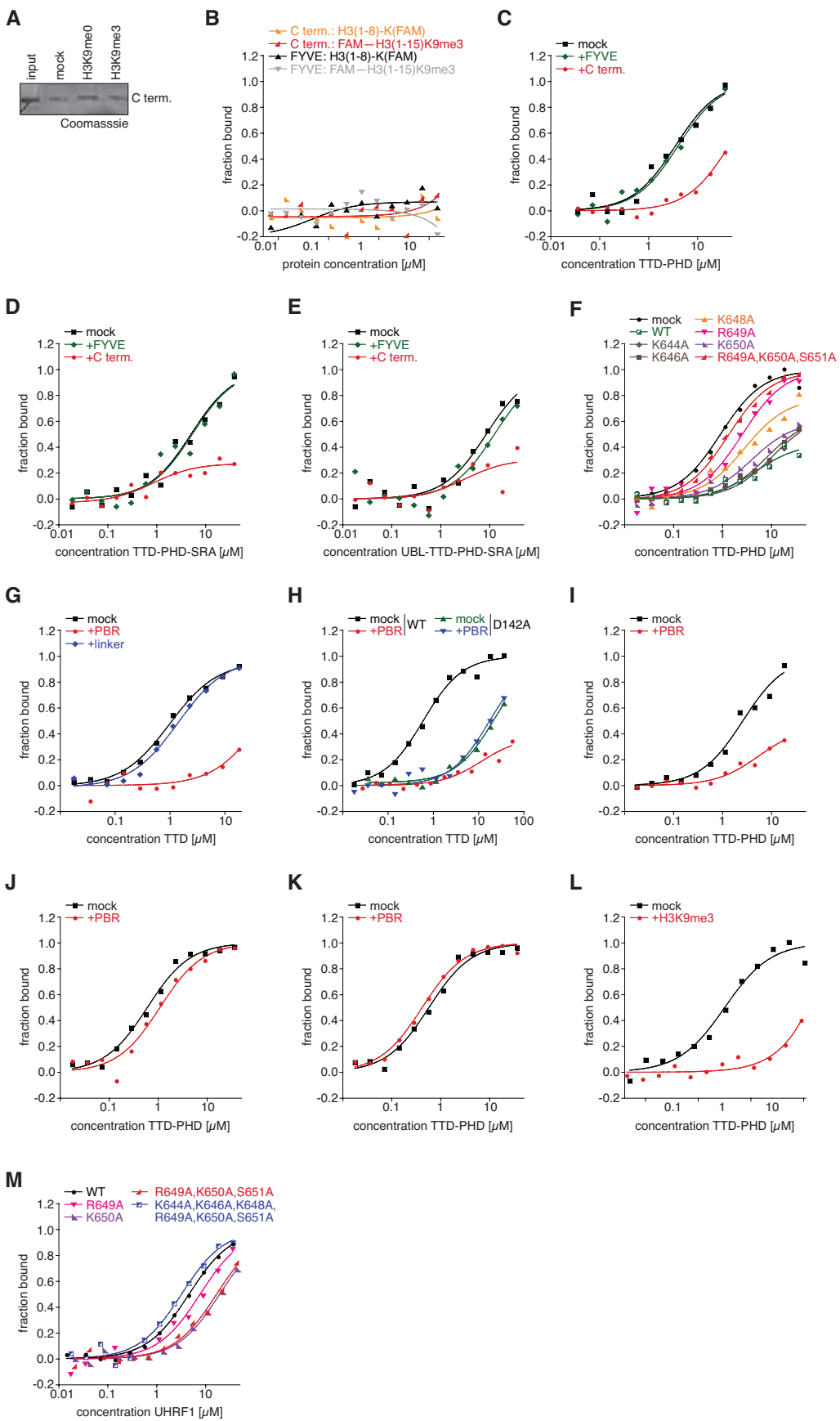


Figure S4. The PBR Sequence within the C Terminus Blocks TTD/H3K9me3 Interaction

Related to Figure 4

- (A) The C terminus of UHRF1 was incubated with the specified biotinylated H3(1-20) peptides immobilized on streptavidin magnetic beads. Mock represents pull-down with beads only. Recovered material was analyzed by Coomassie staining. Input, 2%.
- (B) The C terminus of UHRF1 or the FYVE domain of Eea1 were analyzed in fluorescence polarization binding experiments using the indicated fluorescein-labeled peptides.
- (C)-(E) The specified fragments of UHRF1 alone (mock) or in presence of the C terminus of UHRF1 or the FYVE domain of Eea1 (1:2 molar ratio) were analyzed in fluorescence polarization binding experiments with a FAM-H3(1-15)K9me3 peptide.
- (F) The TTD-PHD alone (mock) or in presence of the indicated PBR wild-type (WT) or mutant peptides (1:5 molar ratio) was analyzed in fluorescence polarization binding experiments with a FAM-H3(1-15)K9me3 peptide.
- (G) The TTD alone (mock) or in presence of PBR or linker peptides (1:5 molar ratio) was analyzed in fluorescence polarization binding experiments with a FAM-H3(1-15)K9me3 peptide.
- (H) Wild-type TTD (WT) and TTD mutated in the D142 residue within the peptide-binding groove (MT) alone or together with the PBR peptide (1:5 molar ratio) were analyzed in fluorescence polarization binding experiments using a FAM-H3(1-15)K9me3 peptide.
- (I)-(K) The TTD-PHD alone (mock) or in presence of the PBR peptide (1:5 molar ratio) was analyzed in fluorescence polarization binding experiments using FAM-H3(1-15)K9me3 (I), H3(1-15)-K(FAM)K9me3 (J) or H3(1-15)-K(FAM)K9me0 (K) peptides.
- (L) TTD-PHD alone (mock) or in presence of the H3(1-20)K9me3 peptide (1:5 molar ratio) was analyzed in fluorescence polarization binding experiments using fluorescein labeled PBR peptide.
- (M) Wild-type UHRF1 (WT) or UHRF1 carrying the indicated mutations were analyzed in fluorescence polarization binding experiments with a H3(1-8)-K(FAM) peptide.

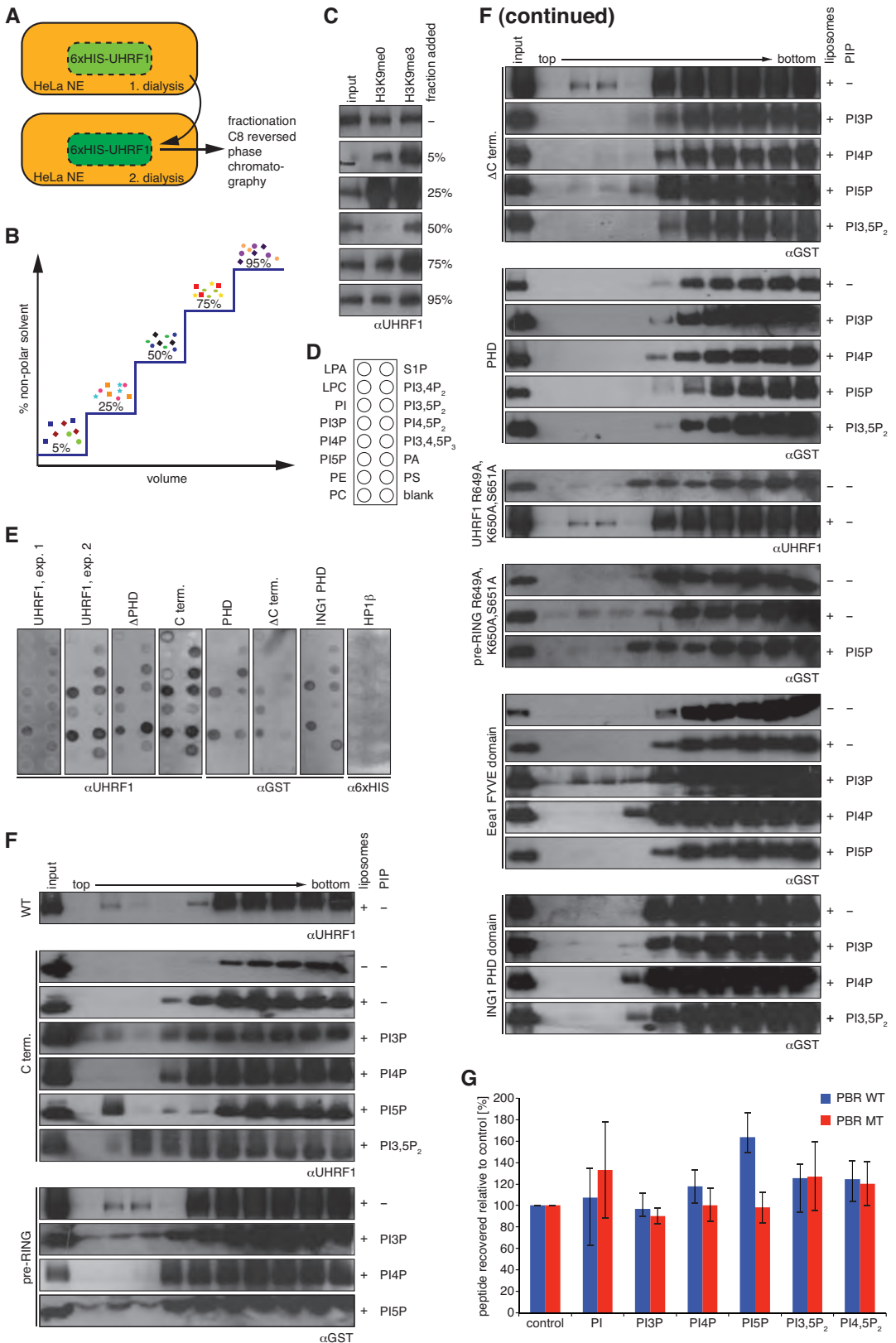


Figure S5. The PBR Sequence of UHRF1 Interacts with PI5P

Related to Figure 5

(A) Flow scheme of the dialysis and purification experiment for enrichment of the cellular cofactors of UHRF1.

(B) Fractionation scheme of the cellular components enriched with UHRF1 protein or UHRF1 fragments after dialysis against HeLa NE on a C8 reversed phase column.

(C) Fractions from the dialysis and purification scheme depicted in (A) and (B) using wild-type UHRF1 protein were lyophilized. Recombinant UHRF1 incubated with the different fractions was analyzed in pull-down experiments using the specified biotinylated H3(1-20) peptides immobilized on streptavidin magnetic beads. Recovered material was analyzed by western blot. Input, 2%.

(D) Layout of the lipid dot blot. LPA, lysophosphatidic acid; LPC, lysophosphatidylcholine; PI, phosphatidylinositol; PI3P, phosphatidylinositol 3-phosphate; PI4P, phosphatidylinositol 4-phosphate; PI5P, phosphatidylinositol 5-phosphate; PE, phosphatidylethanolamine; PC, phosphatidylcholin; S1P, shingosin 1-phosphate; P3,4P₂, phosphatidylinositol 3,4-bisphosphate; P3,5P₂, phosphatidylinositol 3,5-bisphosphate; P4,5P₂, phosphatidylinositol 4,5-bisphosphate; P3,4,5P₃, phosphatidylinositol 3,4,5-trisphosphate; PA, phosphatidic acid; PS, phosphatidylserine.

(E) The indicated proteins were incubated with lipids spotted on a nitrocellulose membrane according to the scheme in (E). Retained material was analyzed by western blot. ΔPHD and ΔC terminus correspond to the UHRF1 UBL-TTD~SRA-RING and UBL-TTD-PHD-SRA fragments, respectively. The PHD domain of ING1 and HP1β protein served as controls.

(F) The indicated wild-type proteins and protein fragments or mutant proteins and protein fragments were incubated with liposomes containing the indicated PIPs (see scheme of Figure 5E). Fractions of the liposome floatation assay after centrifugation were analyzed by western blot. The FYFE domain of Eea1 and the PHD domain of ING1 served as control. WT, wild-type UHRF; ΔC terminus, UBL-TTD-PHD-SRA; input, 5%.

(G) Fluorescein labeled wild-type (WT) or R649A,K650A,S651 mutant (MT) PBR peptides were incubated with the indicated biotinylated PIPs immobilized on agarose beads. Fluorescence signals after washing were recorded in 96-well plates and normalized to control without lipids. Error bars correspond to SD.

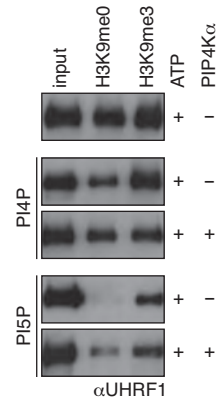


Figure S6. PIP4K α Inhibits the Allosteric Regulation of UHRF1 by PI5P

Related to Figure 6

UHRF1 alone or together with PI4P or PI5P was incubated with the indicated combinations of PIP4K α and ATP. The protein was then analyzed in pull-down reactions with the specified biotinylated H3(1-20) peptides immobilized on streptavidin magnetic beads. Recovered material was analyzed by western blot. Input, 2%.

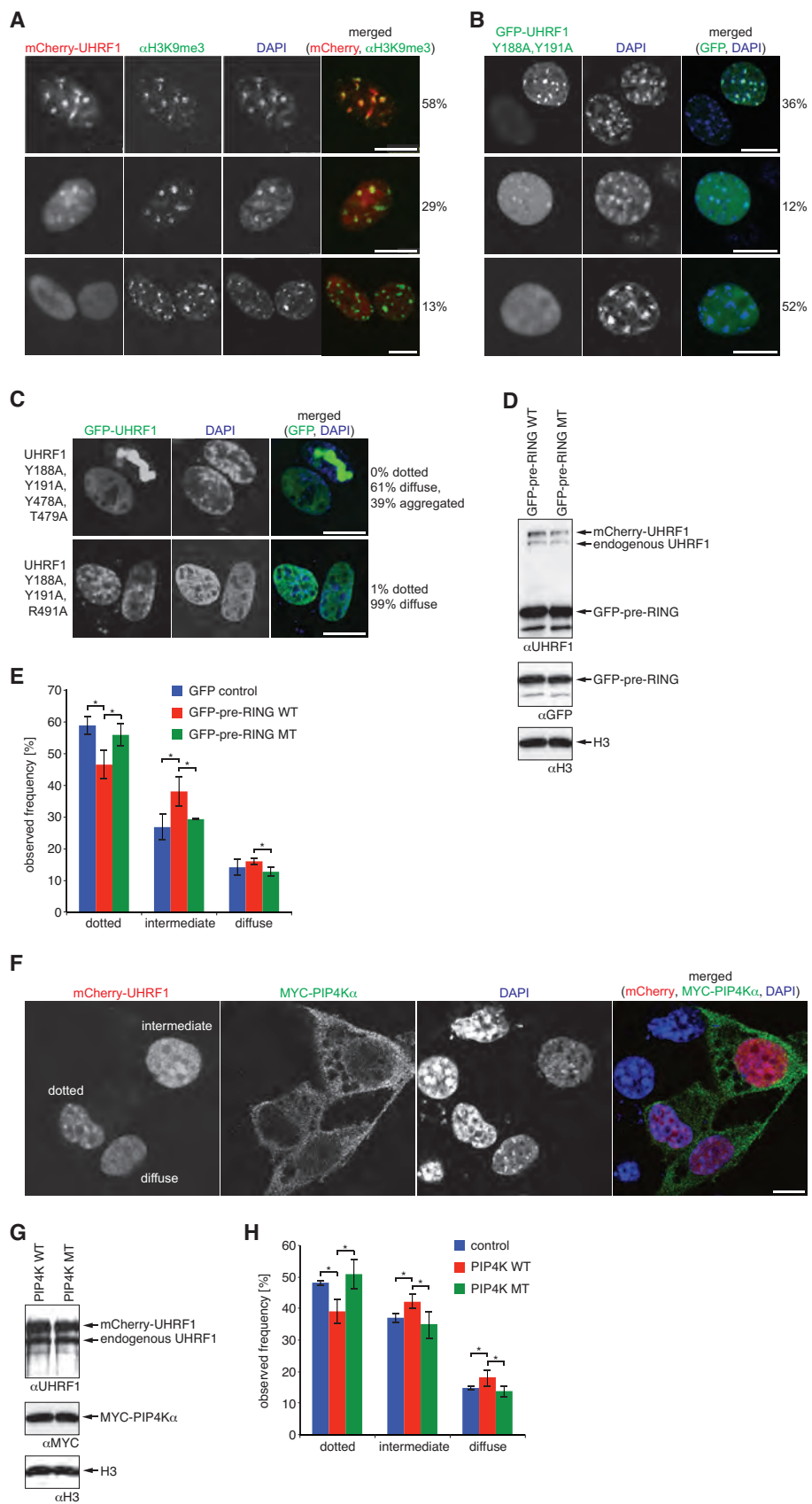


Figure S7. Nuclear Localization of UHRF1 is Regulated by the PBR and PI5P

Related to Figure 7

- (A) mCherry and anti-H3K9me3 immunofluorescence signals of NIH3T3 cells transiently expressing mCherry-UHRF1. Images of representative cells of different phenotypes observed at the indicated frequency ($n > 500$) are shown. DAPI was used to stain DNA. Scale bar, 10 μm .
- (B) and (C) NIH3T3 cells were transfected with the indicated constructs. Fluorescence signals were analyzed by confocal microscopy. Images of representative cells of different phenotypes observed at the indicated frequency ($n > 500$) are shown. DAPI was used to stain DNA. Scale bar, 10 μm .
- (D) NIH3T3 cells were transfected with mCherry-UHRF1 together with GFP-pre-RING wild-type (WT) or GFP-pre-RING K644A,K646A,K648A,R649A,K650A,S651A (MT) constructs. Total cell lysates were analyzed by western blotting.
- (E) Frequencies of different nuclear distribution of mCherry-UHRF1 coexpressed with GFP control, GFP-pre-RING wild-type (WT) or GFP-pre-RING K644A,K646A,K648A,R649A,K650A,S651A (MT) in NIH3T3 cells ($n > 500$). Error bars represent SD of three independent experiments. Asterisks indicate significance intervals of $p < 0.05$ determined by a two-tailed Student's t-test.
- (F) mCherry and anti-MYC immunofluorescence signals of NIH3T3 cells transiently expressing mCherry-UHRF1, MYC-PIP4K α and untagged PIP4K β . Cells with different distribution of the mCherry signal are indicated. DAPI was used to stain DNA. Scale bar, 10 μm .
- (G) NIH3T3 cells were transfected with mCherry-UHRF1 together with MYC-PIP4K α and untagged PIP4K β (PIP4K WT) or MYC-PIP4K α G131L,Y138F and untagged PIP4K β D278A (PIP4K MT). Total cell lysates were analyzed by western blotting.
- (H) Frequencies of different nuclear distribution of mCherry-UHRF1 coexpressed with MYC-PIP4K α and untagged PIP4K β (PIP4K WT) or MYC-PIP4K α G131L,Y138F and untagged PIP4K β D278A (PIP4K MT) in NIH3T3 cells ($n > 500$). Error bars represent SD of three independent experiments. Asterisks indicate significance intervals of $p < 0.05$ determined by a two-tailed Student's t-test.

SUPPORTING TABLES

Table S1. Apparent Dissociation Constants of Wild-Type and Mutant UHRF1 Proteins Determined by Fluorescence Polarization Measurements Related to Figures 1-5

	FAM-H3(1-15)		H3(1-15)-K(FAM)		H3(1-8)-K(FAM)
	K9me0	K9me3	K9me0	K9me3	
TTD	nb	1.0 ± 0.2	nb	0.6 ± 0.2	—
TTD Y188A,Y191A	nb	nb	—	—	
PHD	nb	nb	0.1 ± 0.1	0.1 ± 0.05	2.3 ± 0.3
TTD-PHD	nb	4.9 ± 1.0	1.0 ± 0.3	0.5 ± 0.2	—
TTD-PHD-SRA	nb	4.6 ± 3.0	—	—	—
UBL-TTD-PHD-SRA	—	6.5 ± 3.5	—	—	>100
UHRF1 (UBL-TTD-PHD-SRA-RING)	nb	nb	1.5 ± 0.3	0.5 ± 0.2	4.5 ± 2.0
UHRF1 {2x HeLa NE}	nb	2.6 ± 1.7	>100	4.1 ± 2.0	—
UHRF1 D334A,D337A	—	—	—	nb	nb
UHRF1 R649A	—	44 ± 11	—	—	7.7 ± 3.0
UHRF1 K650A	—	nb	—	—	19 ± 5
UHRF1 R649A,K650A,S651A	—	27 ± 8	—	—	17 ± 7
UHRF1 K644A,K646A,K648A, R649A,K650A,S651A	—	8.0 ± 2.2	—	—	3.2 ± 1.2
C terminus	—	nb	—	—	nb

All values given in μM ; nb, not binding (curves did not even get near inflection point); >100 , faithful determination of K_D not possible since curves barely reach inflection point; —, not measured.

Table S2. Apparent Dissociation Constants of Wild-Type and Mutant TTD and TTD-PHD Fragments Determined by Fluorescence Polarization Measurements

Related to Figures 1-5

	TTD WT	TTD D142A	TTD Y188A, Y191A	TTD-PHD WT	TTD-PHD R295A, R296A
PBR WT	3.5 ± 1.9	nb	13 ± 4	3.5± 1.6	4.3 ±1.8
PBR K644A	4.9 ± 1.6	—	—	—	—
PBR K646A	4.3 ± 1.4	—	—	—	—
PBR K648A	61 ± 8	—	—	—	—
PBR K649A	nb	—	—	nb	—
PBR K650A	19 ± 5	—	—	92 ± 21	—
PBR R649A, K650A,S651A	nb	—	—	nb	—
linker	nb	—	—	>100	30 ± 9

All values given in μM; nb, not binding (curves did not even get near inflection point); >100, faithful determination of K_D not possible since curves barely reach inflection point; —, not measured.

EXTENDED EXPERIMENTAL PROCEDURES

Plasmids

All cloning was done according to standard procedures. Mutagenesis was performed using the QuickChange protocol (Stratagene). Details are available upon request. All clones are based on human UHRF1 cDNA (NM_001048201). For expression in *E. coli* : pETM13 UHRF1(aa 1-793)-6xHIS; petM40 MBP-UHRF1(aa1-793)-6xHIS; pET16 10xHIS-TTD(aa 126-285), pGEX4T3 GST-PHD(aa298-366)-10xHIS; pET16b 10xHIS-TTD-PHD(aa 126-376); pETM13 TTD-PHD-SRA(aa 126-605)-6xHIS; pETM13 UBL-TTD-PHD-SRA(aa 1-619)-6xHIS; pETM13 C terminus(aa 605-793)-6xHIS; pETM13 preRING(aa 605-675)-6xHIS, pETM13 UBL-TTD~SRA-RING(aa 1-309,371-793)-6xHIS; pETM13 UBL-TTD~SRA(aa 1-309,371-619)-6xHIS. For expression in Sf9 cells: pFastbac1 6xHIS-UHRF(aa1-793). For expression in mammalian cells: pcDNA3.1 UHRF1(aa1-793)-2xHA2xFLAG, pEGFP-C1 UHRF1(aa1-793), pEGFP-C1 UHRF1(aa1-793) R491A, pEGFP-C1 UHRF1(aa1-793) Y188A,Y191A, pmCherry UHRF1(aa1-793), pmCherry UHRF1(aa1-793) R491A, pmCherry UHRF1(aa1-793) Y188A,Y191A, pEGFP-C1 pre RING (aa 605-675), pEGFP-C1 pre RING (aa 605-675) K644A,K646A,K648A,R649A,K650A,S651A. pcDNA3.1 MYC-PIP4K α and pcDNA3.1 PIP4K β have been described (Bultsma et al., 2010). Mutant kinases were PIP4K α G131L,Y138F and PIP4K β D278A in the same backbone. The plasmid for expression of GST-FYVE domain of Eea1 was a gift of Harald Stenmark (Oslo University), the plasmid for expression of 6xHIS-PHD domain of ING1 was a gift of Tatiana Kutateladze (University of Colorado).

Peptides

Peptides were synthesized using Fmoc chemistry on an Intavis Ressep XL synthesizer. TentaGel R RAM resin (cap.: 0.18 mmol/g) served as solid support and the amino acid side-chains were protected as follows: Arg(Pbf), Asn(Trt), Asp(OtBu), Cys (Trt), Gln (Trt), His(Trt), Lys(Boc), Ser(tBu), Thr(tBu), Trp(Boc), Lys(Me₃) and Lys(Mtt) for orthogonal deprotection of the ϵ -amino group. Coupling reactions

were performed with 2-(1H-benzotriazole-1-yl)-1,1,3,3-tetramethyluroniumhexafluorophosphate (HBTU) as coupling reagent and N-methylmorpholine (NMM) in DMF/NMP as base. Lys(me3) was introduced manually with PyOxim (Ethyl cyano(hydroxyimino)acetato-O²]tri-1-pyrrolidinylphosphonium hexafluorophosphate) at the indicated positions. N-terminal labeling of H3-derived peptides was performed with fluorescein using 5-Carboxyfluorescein, Succinimidyl Ester. 5,6-Carboxyfluorescein was coupled at the N-terminal amino group of peptides derived from PBR with PyOxim on solid support. 5,6-Carboxyfluorescein was coupled at the ε-amino group of C-terminal Lys residues using HBTU/Hydroxybenzotriazole (HOBr) and NMM in DMF. Pseudoproline dipeptides were used for efficient synthesis of H3 and PBR-derived peptides. Peptides were cleaved off the resin with TFA:Phenol:Triisopropylsilane:H₂O (85:5:5:5) for four hrs. All peptides were purified by reversed phase C18 HPLC and verified by ESI- and MALDI-MS. Peptide backbones; methylated residues are indicated in bold: H3(1-8)-K(FAM) = ARTKQTAR-K(ε-amino-FAM); FAM-H3(1-15) = α-amino-FAM-ARTKQTARKSTGGKA; H3(1-15)-K(FAM) = ARTKQTARKSTGGKA-K(ε-amino-FAM); H3(1-20)-K(biotin) = ARTKQTARKSTGGKAPRKQL-K(ε-amino-biotin); FAM-PBR WT = α-amino-FAM-GKGKWKRKSAGGGPS; FAM-PBR K644A = α-amino-FAM-GAGKWKRKSAGGGPS; FAM-PBR K646A = α-amino-FAM-GKGAWKRKSAGGGPS; FAM-PBR K648A = α-amino-FAM-GKGKWARKSAGGGPS; FAM-PBR R649A = α-amino-FAM-GKGKWKRASAGGGPS; FAM-PBR R649A,K650A,S651A = α-amino-FAM-GKGKWKRKSAGGGPS; FAM-linker = α-amino-FAM-VDNPMRRKSGPSCKH; PBR-K(biotin) = GKGKWKRKSAGGGPS-K(ε-amino-biotin); linker-K(biotin) = VDNPMRRKSGPSCKH -K(ε-amino-biotin). For competition experiments biotinylated peptides were used.

Antibodies

Western blotting: anti-UHRF1 (Santa Cruz sc-373750, 1:5000 and sc-100606, 1:1000), anti-GST (Santa Cruz sc-138, 1:1000), anti-6xHIS (Santa Cruz, sc-57598 1:500), anti-FLAG (Sigma F3165, 1:1000 and Santa Cruz sc-807, 1:1000), anti-MYC (Abcam ab-9106, 1:5000), anti-H3 (Abcam ab-1791,

1:10000), anti-GFP (Santa Cruz sc-9996, 1:2000).

Immunoprecipitation: anti-UHRF1 (Santa Cruz sc-373750, 1:1000), anti-GST (Santa Cruz, sc-138, 1:500).

Immunofluorescence: anti-MYC (Abcam ab9103, 1:500) anti-H3K9me3 (Active Motif 39161, 1:1000), anti-rabbit IgG Alexa 488 (Invitrogen A21206, 1:500).

Protein Expression and Purification

Proteins were expressed in BL21-RIL *E. coli* cells or Sf9 insect cells using standard procedures (details are available upon request). HIS-tagged proteins were purified on HisPur Cobalt resin (Pierce) and GST tagged-proteins were purified on glutathione sepharose (GE Healthcare) according to manufacturers' protocols. Eluates from the resins were dialyzed into 50 mM Tris-HCl pH 8, 150 mM NaCl, 10% v/v glycerol, 1 mM DTT and concentrated using ultracentrifugation (Amicon). HEK293 cells were grown in DMEM Glutamax II (supplemented with pen/strep, glutamine, and BGS) and transfected using a Calcium-Phosphate transfection kit (Clontech). After lysis FLAG-UHRF1 was purified on sheep-anti-mouse Dynabeads (Invitrogen) loaded with anti-FLAG antibody. After 2 hrs at 4°C, beads were washed twice with SP buffer (50 mM Tris-HCl pH 8, 100 mM NaCl) and once with the same buffer but 500 mM NaCl. Protein was eluted twice in 15 µl FLAG peptide (Sigma, 5 µg/µl in SP buffer).

Peptide Pull-downs

40 µl streptavidin paramagnetic beads (MagneSphere, Promega) were washed three times with PBS in low-binding tubes. 10 µg biotin-labeled peptide or water was added for 2 hrs at 4°C with rotation followed by three washes with PBS. 10 µg recombinant proteins in 500 µl PD300 buffer (20 mM HEPES-NaOH pH 7.9, 300 mM KCl, 0.2% v/v Triton X-100, 20% v/v glycerol) were added and incubated three hrs at 4°C with rotation. Beads were washed six times with PD300 and recovered material was eluted in 30 µl PDelute buffer (50 mM Tris-HCl pH 8, 25% v/v glycerol, 0.25% w/v bromophenol blue, 1 mM EDTA, 2% w/v SDS, 1 mM TCEP) by boiling for 5 min. PIP suspension of the lyophilized diC16 forms

(Echelon Biosciences) were made by adding water. Protein was preincubated at 10-fold molar excess of PIPs in PD300 buffer for overnight at 4°C in a low-binding tube. Nuclear extracts of cells were prepared according to published procedures (Osborn et al., 1989) and used at 2 mg total protein per pull-down. Samples were pre-cleared by addition of Triton x-100 to 0.2% v/v, protease inhibitor (Roche complete), and 20 µl pre-washed beads for 2 hrs at 4°C with rotation. For pull-downs using HeLa NE pre-reacted with Phospholipase A2, 100 µg PLA2 (Sigma, bovine pancreas) was added to 1 ml HeLa NE supplemented with 1 mM CaCl₂ and reacted overnight at 4°C. PBR peptides were incubated with 10-fold molar excess of PIP (diC16, Echelon Biosciences) overnight at 4°C. PBR peptides were then applied to beads as above. TTD was loaded with 10-fold molar excess PIP for 3 hrs at 4°C with rotation.

Dialysis of UHRF1

HeLa cells were grown in fermenters, harvested, washed with PBS and flash frozen in liquid nitrogen. Nuclear extracts were prepared according to the Dignam protocol with final dialysis in buffer C (20 mM HEPES pH 7.9, 20% v/v glycerol, 100 mM KCl, 0.2 mM EDTA, 0.5 mM DTT) (Dignam et al., 1983). Extracts were clarified by high speed centrifugation, aliquoted and stored at -80°C for further use. Protein concentration ranged from 10-15 mg/ml.

Proteins (5 mg in 400 µl) were dialyzed against 10 ml HeLa NE or comparable buffer (in 50 ml tubes) overnight in dialysis cups (Pierce) with 3500 Da molecular weight cut-off at 4°C. Solutions were clarified by high speed centrifugation and protein concentration was spectrophotically determined. For sequential dialysis MBP-UHRF1 was dialyzed against 6xHIS-UHRF1 that had been treated as described above.

For pull-downs using HeLa NE pre-reacted with PIP4Kalpha: HeLa NE was incubated with recombinant PIP4Kα supplemented with ATP or ATPγS, and MgCl₂ (all 1 mM final concentration), for 8 hrs at room temperature. Addition of ATP and MgCl₂ resulted in massive protein degradation in the extracts, preventing analysis of endogenous UHRF1. Therefore purified UHRF1 was dialyzed against the PIP4Kα-treated extracts.

Fluorescence Polarization

Fluorescence polarization (FP) experiments were performed and analyzed as described in FP buffer (25 mM Tris pH 7.5, 50 mM NaCl, 5% v/v glycerol) using a HIDEX Chameleon II plate reader at 4°C (Fischle et al., 2008). For UHRF1 dialyzed against HeLa NE or buffer: Full-length UHRF1 was dialyzed twice against 10 ml of HeLa nuclear extract or comparable buffer overnight at 4°C. Protein was used for fluorescence polarization measurements after concentration determination, without any further treatment. For competition FP experiments: Purified proteins were pre-incubated with non-labeled competitor peptide or protein domain at the indicated molar ratios for 30 min at 4°C. For all experiments shown signals from multiple measurements ($n > 3$) were normalized, averaged and plotted.

Analytical Ultracentrifugation

Double-sector charcoal filled epon cells were loaded with 412 µl of sample buffer or 392 µl protein sample at 0.5 OD₂₈₀ of recombinant UHRF1, either dialyzed against HeLa NE or buffer. Samples were equilibrated in the Beckman XL-A analytical ultracentrifuge 2 hrs to 20°C under vacuum, prior to starting the run. During the run at 50,000 rpm, scans were continuously acquired until all material was at the bottom of the cell. Data analysis was performed with the SEDFIT software using a calculated partial specific volume of 0.722 ml/g for recombinant UHRF1 (Schuck and Rossmanith, 2000). Generally, after positioning the meniscus and the bottom, a simplex fit for the meniscus position was performed at a resolution of 200. The frictional ratio was fitted with the simplex algorithm. Initial values were further refined by fitting with the Marquard-Levenberg and simulated annealing algorithms until the root mean square deviation converged at a minimum. Final fitting was done with a resolution of 200 for the sedimentation coefficient. To address sedimentation coefficient and frictional ratio distribution of the sedimenting UHRF1 population, the continuous C(S)/ff0 distribution model was used at a resolution of 100 for C(S) and 10 for the frictional coefficient (range 1-2.5).

Co-immunoprecipitation

10 µl Dynabeads (Invitrogen) were washed once with PBS, twice with IP150 buffer (50 mM Tris pH 8, 150 mM NaCl, 5% v/v glycerol, 0.05% v/v Triton x-100), and resuspended in IP150 buffer supplemented with 5% w/v BSA. 0.22 nmoles protein were mixed with 1 µl anti-UHRF1 antibodies in 100 µl IP150 buffer, 5% w/v BSA. After 30 min incubation at 4°C, 10 µl washed beads were added and the reactions were rotated at 4°C for 2 hrs. 0.22 nmoles TTD was then added for three more hrs. Reactions were washed five times with IP150 buffer, and eluted using 30 µl PDelute buffer (see above). Samples were evaluated by SDS-PAGE and western blotting. For immunoprecipitations with added H3 competitor peptide, TTD was pre-incubated with H3 peptides at 1:2.5, 1:5, and 1:7.5 molar ratio for 30 min. For immunoprecipitations with added PIPs as competitor, the steps outlined above were followed, with two changes. C terminus and PIPs or water were incubated overnight at 4°C, at a molar ratio of 1:5, 1:10, and 1:20, before mixing with anti-UHRF1 antibody. The detergent was omitted in the IP150 buffer.

Isothermal Titration Calorimetry

TTD and C terminus were dialyzed two times together but in separate dialysis tubing against 1 l filtered (0.45 µm) DITC buffer (20 mM Tris pH 8.0, 100 mM NaCl). Used DITC buffer was de-gassed and retained for washing the ITC sample cell and for ITC control buffer/protein runs. Proteins were concentrated, filtered (0.45 µm) and used for ITC measurements in an ITC-200 (MicroCal) pre-equilibrated to 20°C. The C terminus was added to the sample cell at 50 µM, while the TTD was loaded in the syringe at 500 µM. ITC injection conditions were: 20 injections, 20°C, reference power = 7, 120 second initial delay, spinning = 700-1000, feedback = high. The first injection was 0.2 µl, 0.4 sec duration, 120 sec delay, and the following 19 injections were 2 µl, 4 sec duration, 150 sec delay. The first injection was excluded from the data analysis. Baselines of resulting spectra were adjusted to zero, with buffer/protein reference titrations (having negligible signal) subtracted from protein-protein curves. Curves were evaluated and fits were generated using the software associated with the MicroCal instrument.

PIP Dot Blots

PIP strips (Echelon Biosciences) were blocked with 5 mL PBS-B (PBS, 3% BSA (fatty acid free)) at room temperature for 1 hr. Strips were incubated overnight at 4°C with 5 µg of purified protein in 5 ml PBS-B followed by three washes, 10 min each in 10 ml PBS-T (PBS, 0.1% v/v Tween-20). Reactions were developed by incubation with primary antibody diluted in 5ml PBS-B for 1 hr at 4°C. Membranes were washed three times with 10 ml PBS-T, and then incubated for 1 hr in 5 ml PBS-B with secondary antibody. Strips were washed three times in 10 ml PBS-T, developed with ECL reagent (GE Healthcare) and exposed to film.

Liposome Flootation Assay

10 µl of Poly-piposomes (Echelon Biosciences) were incubated with 0.5 nmoles purified UHRF1, for 10 min on ice. The protein/piposome mixture was filled to 300 µl with cold flotation buffer (50 mM Tris-HCl pH 8, 150 mM NaCl), and mixed with 200 µl cold 75% sucrose in flotation buffer. The mixture (final concentrations 30% sucrose, 1 µM PIP, 1 µM UHRF1, 20 µM liposomes) was applied to a thick-wall polyallomer 11 x 34 mm centrifuge tube (Beckmann). The second layer of the gradient, 400 µl 25% sucrose in flotation buffer, was applied without disturbing the bottom layer. The top layer, 100 µl flotation buffer, was applied without disturbing the middle layer. Tubes were centrifuged for one 1 hr, 55,000 rpm at 4°C, in a TLS-55 swinging bucket rotor (Beckmann). 100 µl fractions were collected from the top of the tube using a pipette, and 15 µl of each fraction was analyzed by SDS-PAGE and western blotting.

Binding of PBR Peptides to PIP Beads

PBR peptides labeled with fluorescein, either WT or R649A-K650A-S651A mutant, were used for PIP bead pull-downs. 10 µl slurry of PIP beads (Echelon Biosciences, control/PI/PI3P/PI4P/PI5P/PI34P/PI35P/PI45P/PI345P) was washed in low-binding tubes twice with binding buffer (10 mM HEPES-NaOH pH 7.9, 150 mM NaCl, 0.5% NP40). 20 ng fluorescein labeled

WT or R494A,K650A,S651A PBR peptide in 50 μ l binding buffer were added to the drained beads, and incubated for 2.5 hrs at 4°C in the dark. Beads were then washed four times, using 100 μ l binding buffer each time. Samples were transferred to black 96-well plates (Corning) and fluorescence intensity (excitation at 485 nm, emission at 535 nm) was measured in a HIDEX Chameleon II plate reader. Fluorescence intensities were averaged from three successive reads and recovery of the peptides was normalized relative to the input.

Reversed Phase Fractionation

Dialyzed proteins (~2-3mg) were filtered (0.45 μ m) and applied (1 ml/min) to a preparatory C8 column (Grace Vydac) pre-equilibrated with 5% acetonitrile, 0.1% formic acid in H₂O at room temperature on a Shimadzu HPLC system. A step gradient of 15 min each at 5%-25%-50%-75%-95% acetonitrile in H₂O/formic acid was applied. Fractions corresponding to the different steps were lyophilized, resuspended in 40 μ l dialysis buffer, and incubated overnight with purified full-length UHRF1 (30 μ g) for further analysis using the peptide pull-down assay.

NMR Spectroscopy

Chemical shift changes of the residues of the TTD upon titration of unlabeled linker peptide were mapped using prior available chemical shift assignments deposited in the BMRB (Nady et al., 2011). ¹H-¹⁵N HSQC spectra were collected at 25°C on a Bruker Avance 500MHz spectrometer. Composite chemical shift changes (Δ ppm) were calculated using the equation $((\Delta\text{ppmN}/6.5)^2 + (\Delta\text{ppmHN}^2))^{0.5}$. Histogram profiles were plotted with Microsoft Excel, and figures of TTD with residues corresponding to significant chemical shift changes were generated with PyMol (DeLano Scientific, US).

Molecular Docking

The docking of the PBR peptide to the TDD was performed using HADDOCK v2.1 software (de Vries et al., 2007; Dominguez et al., 2003). Chemical shift perturbation data were translated into

ambiguous interaction restraints (AIR) to drive the docking process. Residues having both high solvent accessibility and large chemical shift perturbation upon binding, were selected as active residues for AIR. These include residues Y140, E153, D190, E193, R207, I211, F237, W238, and E276. The semi-flexible regions of the TTD were defined automatically by HADDOCK, and all residues in the PBR peptide were set to be flexible. The starting structures for the docking experiment were an extended conformation of the PBR peptide generated with CNS (Brunger et al., 1998), and a conformation of the TTD derived from the TTD-PHD crystal structure (pdb: 3ASK; (Arita et al., 2012)). 5,000 docked structures were calculated, and the 200 best solutions were clustered using 6.5 Å rmsd cut-off. Two models, that represent two best clusters each, were selected for subsequent analysis. The selected models, 1 and 2, have similar HADDOCK-scores, of -109 and -108, respectively.

Immunofluorescence Analysis

NIH3T3 cells were grown on glass cover slips to 50% confluency for transfection. Cells were transfected using Lipofectamine LTX (Invitrogen). For competition experiments pmCherry UHRF1 construct was co-transfected together with a 2-fold excess of pEGFP-C1 PBR constructs (i.e. 1.25µg and 2.5µg per 6-well dish). PIP4K constructs were cotransfected with pmCherry UHRF1 construct at 1:1:1 ratio. All expressions were carried out ON (14-16 hrs).

Cells were washed twice with PBS, fixed with 3.7% v/v formaldehyde in PBS for 10 min and permealized with 0.5% v/v Triton-X-100 in PBS for 5 min. Slides were blocked for 30 min in blocking buffer (2.5% w/v BSA, PBS, 0.05% v/v Tween-20) before incubation for 3 hrs with primary antibodies diluted in the same buffer. Slides were washed three times in wash buffer (PBS, 0.05% v/v Tween-20) and incubated for 1 hr with secondary antibodies. Slides were stained with DAPI (1 µg/ml in wash buffer) and mounted with Vectashield (Vector, #H-1000). Images were taken on a Leica SP5 confocal microscope.

SUPPLEMENTAL REFERENCES

Brunger, A.T., Adams, P.D., Clore, G.M., DeLano, W.L., Gros, P., Grosse-Kunstleve, R.W., Jiang, J.S., Kuszewski, J., Nilges, M., Pannu, N.S., *et al.* (1998). Crystallography & NMR system: A new software suite for macromolecular structure determination. *Acta crystallographica Section D, Biological crystallography* *54*, 905-921.

Osborn, L., Kunkel, S., and Nabel, G.J. (1989). Tumor necrosis factor alpha and interleukin 1 stimulate the human immunodeficiency virus enhancer by activation of the nuclear factor kappa B. *Proceedings of the National Academy of Sciences of the United States of America* *86*, 2336-2340.